# INITIATION OF EXPLOSIVES BY LOW STRENGTH SHOCKS

Final Technical Report

By

Professor D. Tabor, Dr. J.E. Field, Dr. M.M. Chaudhri,
Dr. R.E. Winter, Dr. W.L. Ng & Dr. S.N. Heavens

June 1974

EUROPEAN RESEARCH OFFICE
United States Army
London W.1, England



Contract Number DAJA 37-73-C-4059

Physics and Chemistry of Solids,
Cavendish Laboratory,
Madingley Road,
Cambridge, England.

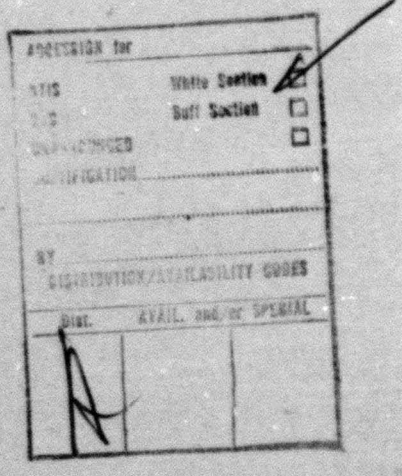
ACCESSION for
NTIS
White Section
Buff Section
UNANNOUNCED
JUSTIFICATION
BY
DISTRIBUTION/AVAILABILITY CODES
Dist. AVAIL. and/or SPECIAL

UNCLASSIFIED

SECURITY CLASSIFICATION OF THIS PAGE (When Data Entered)

i

| REPORT DOCUMENTATION PAGE | | READ INSTRUCTIONS BEFORE COMPLETING FORM |
|---|---|---|
| 1. REPORT NUMBER | 2. GOVT ACCESSION NO. | 3. RECIPIENT'S CATALOG NUMBER<br>AD/A-006209 |
| 4. TITLE (and Subtitle)<br>Initiation of explosives by Low Strength Shocks | | 5. TYPE OF REPORT & PERIOD COVERED<br>FINAL<br>July 1973 - June 1974<br>6. PERFORMING ORG. REPORT NUMBER<br>E-1452 |
| 7. AUTHOR(s)<br>Prof. D. Tabor. Dr. J.E. Field.Dr.M. Chaudri<br>Dr. M.M. Chaudri Dr. W.L. Ng. Dr. S.N. Heavens | | 8. CONTRACT OR GRANT NUMBER(s)<br>DAJA37-73-C-4059 |
| 9. PERFORMING ORGANIZATION NAME AND ADDRESS<br>Department of Physics + Chemistry of Solids<br>Cavendish Laboratory<br>University of Cambridge, Cambridge, ENGLAND | | 10. PROGRAM ELEMENT, PROJECT, TASK AREA & WORK UNIT NUMBERS<br>6.11.02A 20161102B13B 00 276 |
| 11. CONTROLLING OFFICE NAME AND ADDRESS<br>U.S. Army R&D Group (EUROPE)<br>Box 15, FPO New York 09510 | | 12. REPORT DATE<br>JUNE 1974<br>13. NUMBER OF PAGES<br>50 |
| 14. MONITORING AGENCY NAME & ADDRESS(if different from Controlling Office) | | 15. SECURITY CLASS. (of this report)<br>UNCLASSIFIED<br>15a. DECLASSIFICATION DOWNGRADING SCHEDULE |

16. DISTRIBUTION STATEMENT (of this Report)

Approved for public release; distribution unlimited

17. DISTRIBUTION STATEMENT (of the abstract entered in Block 20, if different from Report)

18. SUPPLEMENTARY NOTES

19. KEY WORDS (Continue on reverse side if necessary and identify by block number)

| | |
|---|---|
| (U) Explosives | (U) RDX |
| (U) Shock Initiation | (U) Mass Spectrometry |
| (U) PETN | (U) Drop-weight impact test |
| (U) HMX | (U) Micro-particle initiation |

20. ABSTRACT (Continue on reverse side if necessary and identify by block number)

See over



DD FORM 1 JAN 73 1473 EDITION OF 1 NOV 65 IS OBSOLETE
S/N 0102-014-6601

UNCLASSIFIED
SECURITY CLASSIFICATION OF THIS PAGE (When Data Entered)

This report describes a study of initiative processes involving weak (i.e. kbar strength) shocks. In the period covered by this contract we have done work on the drop-weight impact test, micro-particle initiation of explosives, multiple shocking of samples of PETN and have used mass-spectrometry for decomposition studies of PETN. One of the main features of our drop-weight experiments has been the use of high-speed photography to follow the many processes which take place before initiation starts. The research has emphasized the great importance of the mechanical properties of the explosives in this impact situation. In the micro-particle impact experiments the possibility of localized plastic flow causing initiation has been assessed: the process of flow concnetration by adiabatic shear appears to be important during the impact initiation of some explosives. Multiple shock experiments on PETN show that shock enhancement and sensitization due to fragmentation can be important. The mass spectrometry work on PETN below its melting point showed that sublimation and decomposition occurred concurrently. Decomposition began at about 75°C. The activation energy between 75 and 130° was 45.9 + 1.3 Kcal mole $^{-1}$. In the high mass region a peak at m/e equal to 76 was found. A series of equations for the breakdown of PETN is proposed

## Abstract

This report describes a study of initiative processes involving weak (i.e. kbar strength) shocks. In the period covered by this contract we have done work on the drop-weight impact test, micro-particle initiation of explosives, multiple shocking of samples of PETN and have used mass-spectrometry for decomposition studies of PETN. One of the main features of our drop-weight experiments has been the use of high-speed photography to follow the many processes which take place before initiation starts. The research has emphasized the great importance of the mechanical properties of the explosive in this impact situation. In the micro-particle impact experiments the possibility of localized plastic flow causing initiation has been assessed: the process of flow concentration by adiabatic shear appears to be important during the impact initiation of some explosives. Multiple shock experiments on PETN show that shock enhancement and sensitization due to fragmentation can be important. The mass spectrometry work on PETN below its melting point showed that sublimation and decomposition occurred concurrently. Decomposition began at about 75°C. The activation energy between 75 and 130°C was 45.9 ± 1.3 Kcal mole$^{-1}$. In the high mass region a peak at m/e equal to 76 was found. A series of equations for the breakdown of PETN is proposed.


## Table of Contents

## Introduction

In the research described below we have been particularly interested in the initiation of explosives by impact and by weak (i.e. kbar strength) shocks. The experimental work has developed during the last year in four main areas and these are discussed separately below. In the first area we have investigated the 'drop-weight' impact test which involves dropping a heavy weight on to a sample of explosive; it is a method frequently used for assessing the sensitiveness of an explosive. We have used high-speed photography and pressure measuring techniques for finding out more about the behaviour of samples in this test. This work has shown very clearly the importance of the mechanical properties of the material in determining whether or not initiation takes place.

As explained later micropartical impact studies have practical value and also interest in that a millimeter dimension explosive crystal appears "massive" when impacted by a micron-sized particle. This work has shown that localized plastic flow by adiabatic shear can be important in the impact initiation of some explosives.

The third area of study has involved multiple shocking of PETN. In these experiments the individual shocks were chosen to be too weak to cause initiation alone. The shocks were passed through samples with controlled delays. It appears that under some circumstances the first shock can leave the material more sensitive.

In the final part of the research mass spectrometry techniques have been used to study the thermal decomposition of PETN. It was possible to evaluate the roles played by sublimation and decomposition, and to work out the activation energy for decomposition. Mass spectra of the products were taken of various temperatures, and equations for the breakdown of PETN are proposed.

## 1. The ignition of a thin layer of explosive by impact

### Introduction

A study of the flow properties of thin layers of inert materials subjected to impact is relevant to the problem of the sensitiveness of explosives. One of the standard testing procedures for assessing the hazards involved in handling these materials is to subject a small sample ($\sim$20 - 50mg) of the material to the impact of a falling weight. Repeated series of these tests give some indication of the impact energy necessary to cause ignition, but it is still not known why explosives are ignited by impact. We have used high-speed photographic and pressure-measuring techniques to study the drop-weight impact situation and obtain information on the physical processes occurring that could be responsible for ignition.

In general it is thought that the initiation of an explosive reaction by mechanical shock is thermal in origin, although some workers believe that a tribochemical or a molecular fracture mechanism may be responsible in certain circumstances (Taylor & Weale 1932; Ubbelohde 1948; Fox 1970). On the basis of localized thermal energy or 'hot-spots' as the source of the explosion, four possible mechanisms have been envisaged for ignition by impact.

(i) Adiabatic compression of trapped gas spaces (Bowden, Mulcahy, Vines & Yoffe 1947).

(ii) Viscous heating of material rapidly extruded between the impacting surfaces (Eirich & Tabor 1948; Bolkhovitinov & Pikhil 1958) or by capillary flow between grains (Rideal & Robertson 1949).

(iii) Friction between the impacting surfaces and /or grit particles and/or grains of the material (Bowden & Gurton 1949).

(iv) Localized adiabatic deformation of the thin layer upon mechanical failure (Afanas'ev & Bobolev 1971).

It was shown quite convincingly (Bowden, Mulcahy, Vines & Yoffe 1947) that the presence of gas bubbles affected the impact sensitiveness of nitroglycerine, and Bowden maintained repeatedly (Bowden & Yoffe 1949; Bowden 1950; Bowden & Yoffe 1952; Bowden & Yoffe 1958; Bowden 1963) that mechanism (i) was the primary cause of ignition, not only in liquids but also in solid explosives. This view has with equal persistence been rejected by the Russian school of thought (Andreev, Maurina & Rusakova 1955; Bolkhovitinov 1959; Afanas'ev & Bobolev 1971). In impact experiments on solid explosive materials it was discovered (Kholevo 1946) that the sensitiveness was considerably reduced if the sample was prevented from flowing. Afanas'ev & Bobolev (1961) produced evidence from strain-gauge experiments which suggested that during impact the sample suddenly undergoes a type of fracture. These authors proposed a mechanism of hot-spot formation by the release of energy along slip surfaces formed at the onset of mechanical failure (Afanas'ev & Bobolev 1971; Afanas'ev, Bobolev, Kazarova & Karabanov 1972).

The high-speed photographic experiment described in this report was undertaken in order to provide detailed visual information on the behaviour of a thin layer under impact. The pressure-time measurements, which give qualitative support to Afanas'ev & Bobolev's results, are used together with the photographs to build up a history of the stress and deformation conditions in the layer of material during impact.

## A. High-speed Photography

High-speed photographic observation of the behaviour of the layer of explosive material during impact was achieved with the aid of impacting surfaces of toughened glass, allowing the impact process to be viewed in transmitted light. The arrangement is represented schematically in figure 1. The upper glass block G was held in the recess of the weight W with plasticine. The hardness of the glass was between that of stainless steel and hard steel, and with a fairly high impact energy (5.5kg hammer, 1m drop-weight) it was possible to ignite PETN (pentaerythritol tetranitrate), HMX (octogen, cyclotetramethylene tetranitramine), nitrocellulose, blasting gelatine and ammonium perchlorate, but not RDX (cyclonite, cyclotrimethylene trinitramine), tetryl (trinitrophenylmethylnitramine) or TNT (trinitrotoluene).

The event was photographed at 5μs per frame with an AWRE C4 rotating mirror framing camera, which being of the continuous access type did not require synchronization. The duration of the light flash was fixed at 500μs, less than the period of rotation of the mirror (700μs), so that double exposure on the camera film was avoided.

### Results

**(a) The organic secondary explosives**

A sequence showing the impact of PETN is reproduced in figure 2. The sample is a thin layer of PETN of mass 14mg, and the sequence represents the

final stages of compression of the layer, some 200 s after the initial instant of impact. At this point the layer, which has become compressed to a pellet of almost single crystal density, starts to undergo severe plastic deformation. In frames b-f high-speed (150m/s) jetting occurs and the layer becomes translucent. In frames e and f a wave-like structure can be seen developing within the layer. At frame g the layer suddenly becomes completely transparent and starts to flow very rapidly (300m/s), indicating that the layer has melted. Three ignition sites appear in frame i, followed by growth reaction at 300-400m/s (the central spot D which persists in frames g to i is a defect in the glass; the ignition site I is to the left of this).



RDX showed similar behaviour to that of PETN, but did not reach the stage of melting completely and no ignition sites were observed. One frame from a sequence is shown in figure 18a, in which the partial melting, jetting effect and wave formation can be seen clearly.

Figure 3 shows the behaviour of HMX under the same conditions. This material shows no tendency to melt under impact, but some plastic flow is visible in frame b, following which ignition occurs and a comparatively rapid reaction sets in at 700m/s. However the reaction invariably fails to propagate completely, leaving an unburnt residue (frame f). The residual material is generally at the centre, and the suppression of reaction may be due to the high pressure in this region.

None of the aromatic secondary explosives tetryl, picric acid (trinitrophenol) or TNT could be ignited in the apparatus. These materials showed comparatively little tendency to undergo plastic flow.

(b) Other granular materials

Figure 4 shows selected frames from a sequence on the impact of a layer of ammonium perchlorate. During the early stages of compression the layer gradually becomes transparent (this is probably due to closing up of voids rather than melting, since the same behaviour is observed under static loading. With PETN and RDX the layer does not exhibit the same tendency to become transparent under static pressure as it does under impact). Between frames b and c the layer of ammonium perchlorate suddenly spreads rapidly and loses some of its transparency. This may be the result of a crystalline rearrangement caused by the onset of plastic flow. Following this the jetting effect appears up to frame d, and shortly before frame e ignition of the material takes place, extensive cracking occurs across the layer, and gaseous reaction products are seen escaping through the periphery in frame f. The reaction did not propagate.

None of the other granular solids examined - composition B (60/40 RDX/TNT), gunpowder, ammonium nitrate, silver azide - could be ignited in the apparatus. Ammonium nitrate and gunpowder showed a strong tendency to flow under impact; their behaviour was similar to that of potassium nitrate, which is shown in figure 15. Silver azide and lead azide showed no tendency to undergo plastic flow, and it is probable that their unexpected insensitiveness in this test is peculiar to the perpendicular impact situation (Andreev, Maurina & Rusakova 1955).

**(c) Non-crystalline materials.**

Nitroglycerine, nitrocellulose, blasting gelatine and mining explosives were all found to be sensitive to impact in the glass apparatus. Small drops of nitroglycerine ignited readily even in the absence of air bubbles; ignition occurred at the periphery of the layer and was shown to be almost

certainly due to viscous heating (Heavens 1973). Nitrocellulose showed no tendency to flow under impact, but ignited at a number of sites close to the periphery of the sample, with little tencency for the reaction to propagate. The same behaviour was found with coal-mining explosives. Blasting gelatine showed a rather different behaviour (figure 5), tending to flow steadily like a highly viscous liquid. The material contains a substantial amount of impurity, for example the large grit particle (a chip of wood) protruding from the sample in frame b. Eventually five ignition sites appear (frames d to e) including one at the large wood chip, and examination of the intervening frames showed that all the ignition sites could be identified with small grit particles. Propagation of the reaction at 200-250m/s was relatively complete.

(d) The effect of adding grit to the sample.

When carborundum particles are added to a sample of PETN the resulting behaviour under impact is similar to that of blasting gelatine, a large number of ignition sites being produced. Even a single grit particle can be effective in sensitizing the material and in providing ignition sites. In figure 6 the layer of PETN starts to melt at frame b and the grit particle becomes visible. In frame d ignition occurs at one of the sharp ends of the particle and in the following frame a second ignition site is formed, at the other end. The two ignition sites are probably caused by local stress concentration and plastic deformation of the hard particle at these points. At the time of ignition the average thickness of the layer of PETN is smaller than the thickness of the grit particle (the layer thickness is non-uniform due to the elastic deformation of the impacting glass surfaces), and so the particle is effectively wedged between the impacting bodies. The observation that even with a grit particle present the PETN layer still melts prior to ignition may be significant, suggesting possibly that the melting allows good thermal contact of the material with the hot-spot.

(e) The effect of added wax.

The effect of mixing a small quantity (2-5%) of paraffin wax or inert liquid into samples of PETN and HMX is shown in figures 7 and 8. The layer now exhibits a slowly-spreading viscous fluid-type behaviour not unlike that of blasting gelatine. In both materials ignition occurs close to the periphery of the sample, but the ensuing reaction fails to propagate and is completely extinguished by frame c in both sequences. These observations seem to support the view of Copp & Ubbelohde (1948) that added desensitizers tend to inhibit propagation of the explosion rather than initiation; this effect was attributed by Linder (1961) to thermal insulation by the liquid layers. The tendency to ignite close to the periphery indicates that viscous heating effects may be of some importance.

(f) Impact of ring-shaped samples.

When a layer of granular material is compressed by impact it is possible that air will be trapped inside it. During the early stages of loading most of the air will escape, but if fusion or plastic flow occurs air spaces may be sealed in and compressed. Yoffe (1949) found that if PETN was distributed on the anvil as a ring an increase in the sensitiveness to impact was observed; this effect was attributed to adiabatic heating of the air cavity inside the sample.

Figure 9 shows the impact of a ring-shaped sample of PETN. During compression of the layer the cavity contracts in size and a partially transparent ring-shaped zone is formed (frame b). From frames c onwards the usual

jetting effects and wave patterns are observed, and in frame d the layer starts to melt on the left-hand side. In frame e the layer has melted completely and three ignition sites appear, one of which is close to the point of collapse of the air cavity. This site may be a result of the air pocket being sealed off at the centre of the layer by the ring shaped zone of fused PETN.

Even when the experiment was conducted close to the critical conditions (50% probability) for ignition, ignition sites were observed not only at the air pocket, but also at several other sites. With a very large air cavity, jetting effects are observed within the cavity as well as around the periphery of the sample (Chaudhri, Field, Heavens & Coley 1972). Small air cavities, of diameter 2mm or less, were found to be ineffective in providing ignition sites.

The sensitizing effect of an air cavity was not observed with HMX. In figure 10 it is seen that, because HMX does not melt under impact, the air inside the sample is not sealed off and compressed, but forces its way through the material to the free surface, and ignition does not take place.

(g) Impact of single crystals.

When a single crystal of PETN was subjected to impact, the crystal broke up into a heap of fine powder within 15$\mu$s of the instant of contact of the hammer. Over the next 500$\mu$s the material was steadily compressed to a thin layer, the subsequent behaviour of which was the same as that shown in figure 2. Similarly, variation of the initial grain size of the powdered samples had little influence on their behaviour under impact.

(h) Size effects.

The behaviour of PETN shown in figure 2 occurred only with samples of mass 13mg or more; it was found that in the impact situation examined (5.5kg hammer from a height of 1m) samples of mass 10mg or less invariably failed to ignite. The same effect was observed with HMX, for which the 'critical mass' was about 18mg. Photographic sequences showed that the small samples showed very little tendency to flow.

It is clear that for plastic flow of the sample to occur, the impact pressure must attain the yield strength of the layer $p_y$, which is determined by the uniaxial tensile stress of the material $\sigma_y$ and the thickness h and diameter d of the layer. Application of the Mises yield criterion to a thin layer between two rigid cylindrical punches gives the following relation between these quantities (Schroeder & Webster 1949):

$$p_y = \sigma_y\left[1 + \frac{d}{3\sqrt{3}h}\right] \qquad (1)$$

This indicates that the thinner the layer, the higher the pressure necessary to make the material flow. The variation of ignition probability with layer thickness is considered in detail by Afanas'ev & Bobolev (1971). The size effect is of some importance as it indicates, in accordance with the view of Kholevo (1946), that the sample of explosive must flow plastically before ignition can occur.

## B. Dynamics of impact in the drop-weight test

### Experimental



Pressure-time curves for the impact process were obtained with the aid of a Philips etched-foil resistance-wire strain gauge G (figure 11). The output from the gauge was connected to a Tektronix 551 double-beam oscilloscope, triggered independently by means of an electrical contact made by the falling steel weight W. In experiments with explosive samples the instant of ignition was registered on the second beam of the oscilloscope using either a transient light detector or a simple electrical circuit to detect the explosion.

For accurate calibration of the gauge, and to avoid ambiguity in interpreting the pressure-time curves, it was essential that the impact without a sample should be predominantly elastic in character. This was achieved by using a cast-iron workshop anvil of mass 80kg for the baseplate A; the coefficient of restitution for a hard steel hammer of mass M = 5kg over a range of drop-heights $H_o$ = 0.05 - 1.50m was e = 0.72 - 0.78. Figure 12a shows an oscilloscope trace for impact without a sample. This curve is close to the pressure-time curve calculated from elasticity theory, but because of the incomplete elasticity of the collision the maximum pressure $p_m$ is slightly lower, and the duration of impact $\tau$ marginally longer, than the calculated values.

The gauge was calibrated by equating the impulse measured by the gauge to the momentum change suffered by the hammer:

$$A \int_0^{\tau} p(t)\, dt = MV_o(1 + e) \qquad (2)$$

where $V_o = (2gH_o)^{\frac{1}{2}}$ is the impact velocity, A the area of impact and $p = \alpha U$ the pressure, which is proportional to the voltage signal U from the gauge. The integral was found graphically from the oscilloscope trace. From numerous traces obtained with three drop-weights at varying drop-heights, $\alpha$ was found to be 0.87 $\pm$ 0.03 kbar/mV.

In the steel impact apparatus all the explosive materials except picric acid and TNT could be ignited.

### Results

(a) Impact of inert samples.

When a thin layer of granular material (20-25mg) is inserted between the hard steel rollers R2 and R3, sharp pressure drops are observed on the oscilloscope traces. In figure 12b the pressure rises to 4.5kbar over a period of 80μs and then drops sharply to zero. The pressure drop is not quite instantaneous, but occurs over a time of 5-10μs. From then onwards the trace is approximately sinusoidal in form (apart from the small fluctuations), this stage of the impact process being essentially elastic in character. In figure 12c the pressure drop occurs at a later instant, when the pressure has reached 8kbar, and the elasticity of the collision is substantially reduced. In figure 12d the pressure drop occurs even later, during the unloading stage of the collision. In this event the pressure scarcely rises again after the sharp drop, and the recoil energy of the hammer is almost zero. This type of trace, in which mechanical failure occurs while the pressure is falling, is difficult to account for on the basis of the 'critical stress' hypothesis suggested by Afanas'ev & Bobolev (1971).

For some materials the pressure falls not to zero upon failure but to some finite value (figure 12e). Other materials show not a single sharp pressure drop, but a series of relatively small fluctuations (figure 12f). Materials which are comparatively hard, or possess high melting-points, show no evidence of mechanical failure (figure 12g). In figure 12h is shown an oscilloscope trace for the impact of granular polystyrene, in which the onset of failure is less sudden than for a brittle solid; this could be a manifestation of viscoelastic behaviour. In table 1 is summarized the behaviour of the various materials examined.

(b) Impact of explosive materials.

The solid secondary explosives all showed evidence of mechanical failure during impact. At low impact energies the samples did not ignite and oscilloscope traces similar to figures 12b, c and d were obtained. Above a certain critical impact energy, dependent on the material, the sample ignited, and the lower traces of oscillograms for PETN, HMX, RDX and ammonium perchlorate showed that ignition occurred close to the instant of the sharp drop in pressure (figure 13a).

Sharp drops in pressure during the impact of PETN at the instant of ignition were first observed by Ljungberg (1958), who suggested that the drop in pressure was caused by the explosion, as a result of the rapid expansion of the reaction products or the removal of the layer of material that had been sustaining the pressure. Afanas'ev & Bobolev (1971) also came to the conclusion that the explosion causes the pressure drop, but this interpretation is questionable (and indeed inconsistent with their own theory). Most of the traces obtained by us indicated that the explosion occurs shortly after, or possibly during, the drop in pressure; consequently the pressure drop is due to mechanical failure of the sample, irrespective of whether or not ignition occurs. Figure 13b shows an example of a trace in which the instant of ignition occurs 30μs after the drop. Furthermore, if a relatively large sample was subjected to impact, the explosion destroyed the strain gauge and at the instant of explosion the trace left the scale as in figure 13d. It is clear from this trace that the pressure drop occurred well before the explosion, and that the effect of the explosion was to cause a sharp increase, not decrease, in pressure.

To avoid the possibility of a time lag between the instant of the explosion and the signal from the photocell, an electrical method was substituted, making use of the short-circuit between the steel rollers R2 and R3 resulting from the explosion. With this method a time lag of about 10μs was generally observed between the pressure drop and the explosion (figure 13d).

## Calculation

### The deformation of the sample during impact

The analysis of the pressure-time curves below follows the method adopted by Afanas'ev & Bobolev (1971), and is given here only in outline.

By integrating the oscilloscope trace graphically, the variation in hammer velocity during impact can be found

$$V(t) = V_o - \frac{A}{M}\int_o^t P(t')\,dt' \qquad (3)$$

TABLE 1. THE TYPES OF PRESSURE-TIME CURVES SHOWN BY VARIOUS MATERIALS SUBJECTED TO IMPACT

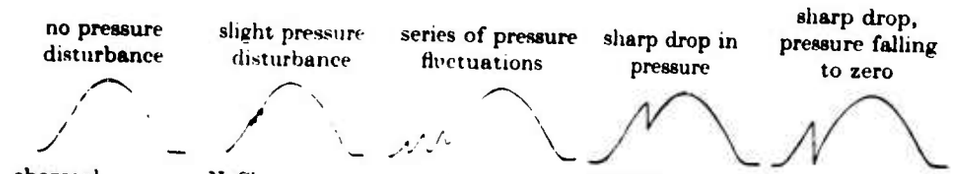

| no pressure disturbance | slight pressure disturbance | series of pressure fluctuations | sharp drop in pressure | sharp drop, pressure falling to zero |
|---|---|---|---|---|
| charcoal | NaCl | tetryl† | $NH_4ClO_4$* | PETN* |
| graphite | KBr | picric acid | $NaN_3$ | RDX* |
| glass | borax | composition B | $BaNO_3$ | HMX* |
| $CaCO_3$ | HgI | oxalic acid | sulphur | TNT |
| $Na_2CO_3$ | polyvinyl alcohol | ammonium oxalate | phenoiphthalein | $NH_4NO_3$ |
| LiF | | ammonium acetate | | $KNO_3$ |
| cellulose (sawdust) | | numerous organic solids | | $KN_3$ |
| NG† | | | | $NH_4Cl$ |
| NC† | | | | tartaric acid |
| blasting† | | | | sucrose |
| gelatine | | | | gunpowder |
| | | | | polystyrene |

* These materials ignited at the instant of the pressure drop.
† These materials ignited, but not at the instant of a pressure drop.

A second integration gives the displacement of the centre of gravity of the hammer, which is effectively a measure of the compressional displacement of the machine components (mainly the steel rollers R1, R2 and R3) and the sample

$$Z_{M+X}(t) = Z_M(t) + Z_X(t) = \int_0^t V(t')dt' \qquad (4)$$

where M refers to the metal and X to the sample. For impact without a sample $Z_X = 0$, and elimination of the time variable from $p(t)$ and $Z_M(t)$ gives a curve for $Z_M(p)$, which for the system of figure 11 is close to linear (24μm/kbar) for the loading part of the impact process. For the unloading stage $Z_M$ does not return to zero at the end of impact and a slightly different curve must be used. This dependence can be used to determine $Z_M(t)$ for the pressure-time curves obtained with a sample, and the sample deformation $Z_X(t)$ can then be determined from equation (4). Finally, the time variable can be eliminated from $Z_X(t)$ and $p(t)$ to give a pressure-deformation curve $p(Z_X)$, from which the energy absorbed by the sample can be calculated. Figure 14 shows one example of a pressure-time curve for impact with a sample, together with the curves $V(t)$, $Z_{M+X}(t)$, $Z_X(t)$ and $p(Z_X)$ derived from it. During the early stages of impact there is often a relatively long slow pressure build-up during which the sample deforms considerably owing to consolidation, while the compression of the steel rollers is small. Towards the end of impact the deformation curve $Z_{M+X}(t)$ represents the elastic unloading of the steel rollers, while the sample undergoes little further deformation; note that $Z_X(t)$ remains roughly constant throughout the later stages of impact.

A sharp pressure drop implies a sharp decrease in the elastic strain $Z_M$ and therefore a sharp increase in $Z_X$, since $Z_{M+X}(t)$ is slowly-varying. Consequently there is an almost discontinuous drop in the thickness of the layer, by an amount 0.1mm for a pressure drop of 5kbar. During the pressure drop the steel components of the impact machine release their stored elastic energy, and much of the sample is extruded or ejected from the impact region.

## Discussion

(a) Interpretation of the pressure drop.

The photographic sequences on the impact of explosive materials described in part A reveal several phenomena - plastic flow, fusion, jetting, wave formation, melting and ignition - with which sharp pressure fluctuations might be expected. To identify which of these processes is associated with a catastrophic drop in pressure, the behaviour of several inert materials under impact was investigated with the photographic system. In figure 15 is shown a sequence on the impact of a sample of potassium nitrate. For a long period (frames a to e) the layer spreads slowly, but over the next 15μs (frames f to h) it suddenly flows rapidly to nearly three times its original area. The jetting effect appears immediately afterwards, in frames h to j. From then onwards the layer ceases to spread any further. The sudden flow of material is demonstrated graphically in figure 16a, in which the mean radius of the layer is plotted as a function of time. Initially the radial flow speed is 6m/s, similar to the velocity of impact, until frame e, when the flow speed increases sharply to 200m/s. It can be shown that this sudden flow of material corresponds to an effectively discontinuous drop in the thickness of the layer. Knowing the mass of the sample, and assuming that the density approaches the single crystal value, the layer

thickness as a function of time can be calculated; this is given by the continuous curve in figure 16b. This curve is close to the behaviour expected from the pressure-time curve for impact of potassium nitrate, the relevant part of which is reproduced as a line diagram in figure 16c. From the p(t) curve the sample deformation $Z_x(t)$ can be calculated as in figure 14, and the variation of the layer thickness is given by

$$h(t) = h_c - Z_x(t) \qquad (5)$$

where $h_o$ is not the initial thickness of the loose sample (0.4mm), but the layer thickness at which substantial loading begins, which is about 40% smaller (Gray 1968). The curve derived from equation (5) is given by the broken line in figure 16b; this diagram shows that the h(t) curves derived from the two experiments are in good agreement.

In this way it has been possible to identify the cause of the pressure drop. When the yield strength of the layer is reached, the material yields plastically and is extruded rapidly between the impacting surfaces (in the impact geometry of figure 11 most of the sample is ejected from the impact area), resulting in a sharp drop in thickness of the layer. The pressure drop occurs during this process, and it is after the pressure has dropped that the jetting effect appears.

Sharp increases in the flow speed of the material immediately prior to jetting were also in evidence with explosive materials. Figure 17 shows a radius-time plot for the impact of a layer of PETN; the first discontinuity AB is due to yielding of the layer, the second CD occurs upon melting.

(b) Energy absorbed by the sample.

From the pressure-deformation curve $p(Z_x)$ the work done on the sample $W_x$ can be calculated. The result can be checked by constructing an energy balance equation

$$W_o = W_{el} + W_{pl} + W_x + W_s \qquad (6)$$

where $W_o$ is the impact energy, $W_{el}$ the elastic energy which is restored to the hammer on recoil and $W_{pl}$ the energy spent on plastic deformation of the machine components. If a sharp pressure drop occurs during impact there is a further loss $W_s$ in the elastic strain energy at that instant. This energy is released in the form of sound waves, which in some experiments were audible as a 'crack' or ringing sound, particularly during trials in which a large energy loss occurred (as in figure 12d). $W_s$ can be calculated, knowing the variation in kinetic energy of the hammer during impact.

A typical example of the energy balance for an impact of the 5kg hammer from a drop-height of 0.25m is

$$W_o = 12.5J, \quad W_{el} = 4.4J, \quad W_{pl} = 3.6J, \quad W_x = 2.9J, \quad W_s = 1.6J$$

In general, about 15-25% of the impact energy is spent on deformation of the sample; at higher impact energies the proportion decreases considerably, and vice versa.

Consequently there is a considerable amount of energy dissipated as heat when the sample undergoes plastic flow. In the case of PETN it is evidently sufficient to melt the sample completely. However, in the glass impact apparatus many of the materials (e.g. TNT) do not undergo plastic flow in bulk. In this event no substantial heat release will occur, and therefore no melting is observed.

(c) Jetting and wave formation in the layer.

In figure 18 are shown single frames from photographic sequences on the impact of layers of RDX and PETN in which wave-like structures are clearly visible. The jet flow in figure 18a is predominantly unidirectional and the waves are formed in parallel straight lines, whereas in figure 18b the jetting is radially symmetric and the wave structure circular. This indicates that the wave formation is closely associated with the jetting effect, the waves lying perpendicular to the direction of flow.

Wave patterns were occasionally observed in the layer of PETN after melting (Figure 18c). The jetting effect was also observed in molten PETN (figure 2, frames h and i) and during the impact of nitroglycerine.

Wave formations have been observed in a number of impact situations, notably explosive welding, and are known to be closely associated with a high-velocity Munroe or 're-entrant' jet at the junction of the colliding surfaces. The formation of a wavy interface is thought to be due to hydrodynamic instability (Hunt 1968), although alternative descriptive mechanisms have been proposed (Cowan & Holtzmann 1963; Bahrani, Black & Crossland 1967). However in the present situation the jetting velocity is not related to the velocity of impact or the angle of skew of impact (which is extremely small), but to the rapid release of strain in the hammer and anvil following mechanical failure of the thin layer. Figures 15 and 17 show that the jetting effect appears immediately after the layer flows plastically, and is the result of material being forced out from the centre of the layer, which in the case of PETN and RDX may be partly molten. The wave formation is caused by the rapid extrusion of this fluid material between the surface of the hammer and the bulk of the layer.

The wave-like structures observed here are not unlike the dark bands observed by Afanas'ev, Bobolev, Kazarova & Karabanov (1972) in thin layers of ferric citrate trihydrate (a complex salt which undergoes an irreversible colour change at 165°C) after impact. These dark bands, which certainly served as evidence of a local high-temperature transition in the material, were interpreted as slip surfaces; however, they bear less resemblance to the slip lines predicted by plasticity theory (Prandtl 1923) than to the wave patterns shown here, which are clearly not slip surfaces formed at the onset of plastic flow, but are a fluid instability effect occurring during jetting.

In the high-velocity welding of metal plates there is evidence of local high temperatures and melting along the wavy interface as a result of trapping of the re-entrant jet and consequent vortex formation (Bahrani, Black & Crossland 1967). Whether such jet trapping is occurring in the present experiment is perhaps doubtful, but the possibility remains that during the rapid extrusion of the jet there is local heating leading eventually to ignition of the material.

The observation that granular samples of PETN melt in bulk prior to explosion is not inconsistent with the proposed ignition mechanism, since there is likely to be a significant thermal induction period, the hot-spots effectively being created before melting of the sample takes place. There is evidence of a long thermal induction period from the central ignition site I in figure 2 (which first appears as a minute spot in frame h) and from the observation that the smaller the sample, the longer is the time lag between melting and ignition. The necessity for melting to occur before the reaction accelerates may be connected with increase in rate of thermal decomposition at the melting-point (Andreev & Kaidymov 1961).

In a few instances a direct connection could be found between the jetting effect and the formation of ignition sites. Pressed pellets of PETN subjected to impact tended to ignite without melting completely (Chaudhri, Field, Heavens & Coley 1972). Figure 19 shows the impact of a pressed sample of PETN containing an air cavity, in which ignition takes place not at the cavity but in the region of severe deformation to one side.

The other possible ignition mechanisms mentioned in the Introduction are unlikely to operate in the present situation. Since plastic flow of the sample in bulk must occur for ignition to be possible, the tribo-chemical, intercrystalline friction and capillary viscous flow mechanisms can be safely dispensed with. As regards viscous heating of the molten PETN during the rapid extrusion following melting (figure 2, frames g to i), calculation gives a temperature rise of only 10°C at the periphery, assuming a value for the viscosity of 0.01 Pa s. The experiments on annular samples of PETN showed that an enclosed air cavity less than 2mm in diameter was ineffective in providing an ignition site, and indeed the compression of small gas spaces by impact is unlikely to be adiabatic (Bolkovitinor 1959). However when jetting occurs it is possible that occluded gas spaces might be compressed during the rapid extrusion of material at 200-300m/s (which is two orders of magnitude higher than the velocity of impact). It is known that gas bubbles as small as 50um can initiate explosion in lead or silver azide if they are collapsed very rapidly (Chaudhri, Field, Heavens & Coley 1972, Chaudhri and Field 1974); bubbles of this size would not be resolved in the present experiments.

## Conclusions

A combination of high-speed photographic and pressure-measuring techniques has enabled the behaviour of thin layers of materials under drop-weight impact to be studied. Various phenomena are revealed, including plastic flow, fusion, jetting, wave formation and melting. With explosive materials ignition occurs at localized sites following severe deformation of the sample.

The compression of gas spaces by impact is effective in causing heating only if they are fairly large and the sample undergoes fusion, allowing the gas cavity to be sealed off. If desensitizers are added, the layer of explosive tends to ignite close to the periphery but the reaction fails to propagate. Added grits sensitize the explosive to impact, hot-spots being formed at sharp points of the grit particle.

When the impacted layer undergoes plastic flow the pressure drops catastrophically and the elastic strain energy in the hammer and anvil is suddenly released, causing the material to be extruded rapidly between the impacting surfaces. The formation of hot-spots, leading to ignition of the material, is thought to occur during the rapid flow process, as a result either of locally obstructed flow or of rapid closure of gas pockets trapped in the material.

A paper on this topic has recently been accepted for publication: S.N. Heavens and J.E. Field, "The Ignition of a Thin Layer of Explosive by Impact" Proc. Roy. Soc. A338, 77-93, 1974.

## 2. Particle impact; the role of localised plastic flow



### Introduction

In these experiments we again studied an impact situation but this time with a very small projectile (micron dimensions).

When devising an impact experiment on a single crystal of explosive the scale of the experiment must be small, partly because of safety factors and partly because large crystals free from macroscopic defects are difficult to prepare. For this reason it was considered advantageous to aim at producing initiation with particles as small as possible. Silver and lead azide were chosen for these studies because these materials have been relatively well studied and because reasonable sized crystals were available. (The crystals were grown in the laboratory and before use they were stored in darkness in a dry atmosphere). The silver azide crystals consisted of flakes of area a few mm with thicknesses in the range 200 to 500μm. The lead azide was in the form of needles a few mm long and with lateral dimensions in the range 50 - 500μm.

Two sets of apparatus were constructed; one employed an electrostatic technique based on a design by Shelton, Hendricks, and Weurker (1960) to accelerate particles in the size range up to 50μm. (see Winter 1971). The velocities to which particles of various sizes accelerated are shown in Figure 20; it can be seen that the smaller particles accelerate to higher velocities. Lead and silver azide crystals were glued to a rigid target rod and impacted by particles with sizes in the range from sub-micron up to 50μm. Increased particle energies were obtained by an explosive driver technique, and the apparatus is shown schematically in Figure 21. Particles of chosen size were placed on a 360μm phosphor-bronze plate below which was a detonator. The sheet was of sufficient thickness not to perforate when the detonator was fired. The acceleration of particles is illustrated in the high-speed photographic sequence of Figure 22: this was taken with a Beckman and Whitley (model 189) camera. From this and similar experiments it was found that for the explosive used (an ICI explosive fuze) the particle velocities were in the range 170 to 220ms$^{-1}$ and did not depend significantly on size and material. For a spall plate to target separation of 10mm, particles placed on the plate with a density of $\sim$ 10 particles/mm$^2$ resulted in $\sim$ 4 impact sites/mm$^2$ on the target.

Initially the explosive crystals were glued to the target rod. However, a possible objection to this was that gas bubbles could be trapped beneath a crystal and during impact these could compress adiabatically and lead to initiation. To prevent this possibility some of the silver azide crystals were mounted as shown in Figure 23 with crystals embedded in an epoxy resin ('araldite') which had been degassed in vacuum. When the 'araldite' had hardened it was polished down to expose a flat face of the crystal. Optical microscopy was used to confirm that gas was not trapped beneath the crystals. All impacts were at normal incidence on regions of the crystal at least twice as thick as the impacting particle diameter. To prevent impacts on thin regions the edges of the crystal were covered with a silicone adhesive compound, which had the added advantage that it caught any particles which landed in it, thus avoiding glancing impacts by reflection of particles from the 'mask'.

Four types of compacted explosive were studied. These were lead azide, silver azide, lead azctetrazol and a mixture consisting of 50% lead dinitroresorcinate, 5% tetrazine and 45% barium nitrate (L-mixture). 20mg portions of these explosives were pressed into 3.1mm diameter aluminium cup under a pressure of 0.14GPa. These specimens were fixed to the target rod so that the exposed face of the powder was impacted.

Glass, aluminium and tungsten spheres were used as projectiles; they were graded into sized lots using sieves.

Initiation Results

(a) Single crystals

For the very small particles which were accelerated by the electrical method the velocities achieved depended on the particle size (see Figure 1). None of these particles caused initiation. However, with the second method larger particles could be fired and it was found that above a critical size particles impacting at $\sim 200 ms^{-1}$ caused initiation of silver azide single crystals. For aluminium and glass particles the critical size was 80 ± 10μm. The crystals were initiated by 40μm tungsten particles, the smallest that could be separated using the available sieves, but not by 10μm tungsten particles (this size range is commercially available). The method of mounting the crystals did not appear to affect their sensitivity to impact initiation.

Crystals impacted by particles near the critical size for initiation but which did not initiate were observed by optical microscopy. (The crystal surfaces deteriorated rapidly making more detailed examination difficult). The impact sites were smooth plastic indentations; only occasional fractures were noticed. Figure 24 shows an indentation of depth about 25μm; this was the deepest observed, indicating that it is close to the critical depth for initiation.

Four lead azide crystals were impacted by 115μm glass particles; two crystals exploded and two did not. The crystals were about 20μm thick and in the cases when initiation was not produced severe fragmentation of the crystals occurred.

(b) Compacted explosives

Aluminium particles were used for these experiments. The critical particle sizes for initiation are shown in table 2. It can be seen that the order of sensitiveness is (i) silver azide and lead azotetrazol (similar) (ii) lead azide (iii) L-mixture.

TABLE 2

Initiation of explosive compacts by aluminium particles impacting at a velocity of $\sim 200 ms^{-1}$.

| Explosive | Critical Particle Diameter (μm) |
|---|---|
| Silver azide | 80 ± 10 |
| Lead azotetrazol | 80 ± 10 |
| Lead azide | 200 ± 30 |
| L-mixture (Lead dinitroresorcinate, Barium nitrate and Tetrazene in the proportions 50, 45, to 5%) | 230 ± 30 |

For all of these compacts the deformation produced by just sub-critical impacts consisted of a depression with a granular surface. Their appearance suggested that a volume of material, about equal to the volume of the impacting sphere, had been dislodged.

## Adiabatic Shear Band Experiments

Winter (1971) suggested that localized adiabatic shear could play an important role in the impact initiation of explosives. A deforming material can develop adiabatic shear bands if two conditions are fulfilled. First, a temperature rise needs to be produced: this will occur if the rate at which heat is generated by plastic flow is greater than that lost by conduction. Secondly, the rate of thermal softening within the bands should be greater than the rate of work hardening. The first experimental study of this phenomenon was made by Zener and Holloman (1944) who used a punch geometry to study the effect of strain rate on the plastic flow of steel. At punch velocities above $3ms^{-1}$ bands of shear were observed within which strains of up to 100 were measured. It was considered that temperatures in excess of 1300K were produced in the bands. Since this early study, adiabatic shear bands have been observed in many materials and for a wide range of deformation situations. For example, Recht (1964) compared the deformation properties of several metals by machining them on a lathe and found that above a critical velocity, adiabatic shear bands appeared in the chips machined from the workpiece. Stock and Thomson (1970) observed shear bands in aluminium alloys which had been impacted with spherical particles and flat-ended cylinders. Microstructural evidence was obtained that melting had taken place in the bands. There is evidence that adiabatic shear can occur in non-metals, particularly if the stress conditions are such that fracture is suppressed by a superimposed hydrostatic pressure. For example, Afanas'ev, Bobolev, Kazarova and Karabanov (1972) impacted compacted ferric citrate trihydrate crystal compacts between anvils and found that dark brown glassy bands appeared in the impacted material. They suggest that melting had taken place along these bands as a result of heat generated by localized flow. There is some evidence that a similar deformation mechanism occurs in rock-like materials during earthquakes (McKenzie and Brune, 1972). Experiments by Andrianova et al (1971) and Roseen (1974) have shown that adiabatic shear can take place in some ductile polymers; in this work large temperature rises in the bands were measured. In recent experiments (to be published) we have shown that when brittle polymers such as polymethylmethacrylate (PMMA) are impacted adiabatic shear bands can be formed having a very similar distribution to those produced in metals.

Because of the small size of the indentations produced by 80μm particles and the explosive nature of the crystal it was impossible to observe whether or not adiabatic shear bands had formed in the impacted silver azide crystals. However, experiments with 80μm particles on PMMA and titanium gave similar impact craters to that illustrated in figure 24. The positions of the shear bands found in titanium impacted with large spheres ( $\sim$ 4mm diameter) are illustrated schematically in Figure 25. In this model, it is assumed that the bands form by a mechanism involving the successive punching of progressively larger diameter cylinders of target material. It is assumed that similar bands could be produced in silver azide when a truly plastic indentation is formed at an impact strain rate. It is therefore suggested that the mechanism responsible for the initiation of silver azide crystals impacted at $200ms^{-1}$ by 80μm Aluminium spheres is the production of high local temperatures as a result of adiabatic shear.

## Conditions for Adiabatic Shear

(a) The mechanisms of initiation

16.

Examination of impact sites in single crystal silver azides formed at sub-critical impact velocities showed that the great majority of the impact energy was used in plastic flow of the explosive. When a material deforms plastically most of the energy of deformation is converted into heat and under impact conditions high temperature pulses can be produced. For example, Yuill (1953) has shown that when a steel needle impacts a rigid plate, flow of the needle can cause a temperature rise sufficient to initiate explosion in a layer of molten cyanic triazide and Uetz and Gommel (1966), using a thermoelectric technique, have recorded temperatures of several hundred degrees when a spherical projectile impacts a rigid steel plate at high velocity.

A difficulty with the plastic flow hypothesis is that calculation shows that if flow is uniform throughout the deforming region, unrealistically high strains are needed to produce temperatures high enough for initiation. However, initiation of an explosive can occur if the energy becomes localized to give a 'hot spot'. Experiments in which non-explosive materials were impacted by spheres have been described; intense localization of flow occurred by a process known as adiabatic shear. The distribution of the shear bands was determined and a model for their formation is proposed. In the analysis which follows this model is used to estimate the conditions under which initiation of explosion by adiabatic shear of silver azide would be expected.

In his study of adiabatic shear during metal cutting, Recht (1964) showed that a critical 'interfacial velocity' is required for the formation of an adiabatic shear band. The critical interfacial velocities for two materials, $V_{c1,2}$, can be approximately compared using the relationship

$$\frac{V_{c1}}{V_{c2}} = \frac{(k\rho c)_1}{(k\rho c)_2} \frac{(\sigma_y)_2^2}{(\sigma_y)_1^2} \left[ \frac{(\partial\sigma/\partial\varepsilon)_1 (\partial\sigma/\partial\theta)_2}{(\partial\sigma/\partial\theta)_1 (\partial\sigma/\partial\varepsilon)_2} \right]^2 \qquad (7)$$

where k is the thermal conductivity, $\rho$ the density, c the specific heat, $\sigma_y$ the flow stress, $\partial\sigma/\partial\varepsilon$ the slope of the stress-strain curve at constant temperature and $\partial\sigma/\partial\theta$ the slope of the stress-temperature curve measured at constant strain. Recht compared the deformation properties of several metals by machining them on a lathe; the geometry in the deforming region is shown in Figure 26. Above a critical machining velocity adiabatic shear bands were found in the chips removed from the workpiece. It is a reasonable assumption that $V_c$ is approximately equal to the critical machining speed. Of the metals tested, Recht found that titanium was most susceptible to adiabatic shear deformation. Using equation (7), the adiabatic shear susceptibilities of silver azide and titanium can be compared to give equation (8). Table 3 summarizes the data at present available for these two materials. The data gives

$$\frac{V_{c_{Ti}}}{V_{c_{AgN_3}}} = 4.7 \left[ \frac{(\partial\sigma/\partial\varepsilon)_{Ti} (\partial\sigma/\partial\theta)_{AgN_3}}{(\partial\sigma/\partial\theta)_{Ti} (\partial\sigma/\partial\varepsilon)_{AgN_3}} \right]^2 \qquad (8)$$

The values for the quantities in brackets are known for titanium, but not for silver azide. However, of the two, silver azide has much the lower melting point and hardness at room temperature (see Table 3).

TABLE 3

| Property | MATERIAL | |
|---|---|---|
| | Titanium | Silver azide |
| Thermal conductivity, k, $Js^{-1}m^{-1}K^{-1}$ | 14 | 3 |
| Specific heat, c, $J\ Kg^{-1}K^{-1}$ | 504 | 500 |
| Density, $\rho$, $Mg\ m^{-3}$ | 4.7 | 5.3 |
| Shear flow stress, $\sigma$, $MNm^{-2}$ | 670 | 150 |
| Melting Point, K | 1953 | 523 |

As the temperature of a solid approaches its melting point temperature softening greatly exceeds any work hardening, $\frac{\partial\sigma}{\partial\theta}$ becomes large and $\frac{\partial\sigma}{\partial\varepsilon}$ small. It seems reasonable that the product of the bracketed terms would be at least unity and possibly higher with the result that $V_{c_{Ti}} \geq 5\ V_{c_{AgN_3}}$. Titanium was shown by Recht to shear adiabatically at $\sim 5mm\ s^{-1}$ and so a velocity of $\sim 1mm\ s^{-1}$ (possibly less) is predicted for silver azide. Any impact situation involving silver azide which produced this order of shear should result in local adiabatic shear deformation.

Given that the conditions for deformation by adiabatic shear are fulfilled the temperature in the shear band can be estimated. Carslaw and Jaeger (1959) present the solution for the temperature rise, $\Delta T$, on a plane in an infinite medium on which heat is generated at a constant rate. If heat is generated on a slip plane at a rate $\sigma V$, where $\sigma$ is the shear stress and V is the velocity of relative movement, then the temperature rise after a time, t, is given by:

$$\Delta T = \sigma V \left(\frac{\tau}{\pi k \rho c}\right)^{\frac{1}{2}} \qquad (9)$$

Taking $\tau = D/V$ where D is the distance moved on the slip plane then,

$$\Delta T = \sigma \left(\frac{DV}{\pi k \rho c}\right)^{\frac{1}{2}} \qquad (10)$$

Since the melting point of silver azide is $\sim 520K$ a value for $\Delta T$ approaching 250K will produce considerable softening. Using the known data for silver azide (see Table 2) we find $DV \sim 4.5 \times 10^{-5} s^{-1}$. In other words if the shear velocity was, for example, $45ms^{-1}$, $\sim 1\mu m$ of relative movement would be required to produce melting.

If melting occurs further heating could take place by viscous flow. Presumably the molten region would 'nucleate' as a very thin layer and then increase in thickness. Simple viscosity theory predicts that the force required to shear a layer of fluid varies inversely as its thickness. An effective shear stress can be estimated using the relationship $\sigma = \frac{\eta V}{t}$ where $\eta$ and t are the viscosity and thickness of the molten film respectively.

Taking t = 5nm (about 8 molecular layers), a velocity of relative movement of 100ms$^{-1}$ and a value for the viscosity of $10^{-3}$Pa s then $\sigma = 2 \times 10^{7}$Nm$^{-2}$. At this flow stress the rate of heat generation on the molten plane would still be significant.

The conclusions are that at high strain rates silver azide, and possibly other explosive materials find it energetically favourable to shear on thin planes in the material where temperature softening (and possibly melting) take place and that temperature rises produced in this way can lead to initiation.

Experiments in which titanium targets were impacted by spherical particles show that the distribution of adiabatic shear bands for this loading geometry is as shown in Figure 25. The bands are assumed to form by a mechanism involving the successive 'punching' of progressively larger diameter cylinders of target material. Here this approximate model is used to estimate the conditions for localized plastic shearing during the impact of silver azide. Assuming that during impact the shear on the most severely deformed plane is by a length D, and that the time $\tau$ to form the impression is the same as the time required to form the indentation (i.e. about 2d/U where d is the depth of the depression and U the velocity of the impacting projectile). Then $V = \frac{DU}{2d}$ where V is the relative velocity across the shear band. It was shown earlier that to produce melting of silver azide

$$DV \geq 4.5 \times 10^{-5} \text{ m}^2 \text{ s}^{-1}$$

$$\text{Thus} \qquad DV \geq 6.7 \times 10^{-1} \frac{2d}{U} \qquad (11)$$

For the just sub-critical indentation shown in figure 24 d $\sim$ 25$\mu$m and U $\sim$ 200ms$^{-1}$, so that the minimum values required by D and V would be 3.4$\mu$m and 13ms$^{-1}$ respectively. Steps of $\sim$3$\mu$m in a crater of $\sim$25$\mu$m depth are clearly feasible (see figure 25 for a schematic drawing showing steps of depth 5$\mu$m in a crater of depth $\sim$25$\mu$m.)

It was assumed in the preceding analysis that slip takes place on the planes at a uniform velocity during the time of formation of the indentation. However, slip would take place first on the planes near the centre of the indentation and then on planes further out. This would make the relative velocity estimated for each plane an under estimate and consequently the required amount of relative slip an over estimate.

In addition to the slip taking place in the bulk of the crystal, relative movement will also occur at the interface between the impacting particle and the crystal. However, the temperature produced here will depend on the thermal conductivity of the impacting sphere and the impacted solid. The fact that the explosive showed similar sensitivities to impact by glass and aluminium spheres, which have thermal conductivities differing by a factor of 250, implies that interface heating was not responsible for initiation.

## Localization of flow in compacted explosives

The observation that plastic flow can produce initiation in the spherical particle impact situation suggests that this mechanism might also be responsible for the initiation of compacted explosives. These consist of many small crystals pressed together; sometimes sensitising grit particles are included. During deformation a large range of stress situations are produced on a micro-scale and there are several deformation processes which could take place leading to localized flow and possibly initiation. Various situations which can be envisaged are depicted in figure 27 (a to m)

and are briefly listed below.

(i) Flow of individual grains

Some grains of explosive will experience large compressive stresses causing plastic deformation. Further localization could take place within individual grains by adiabatic shear processes (figures 27(a) and (b).)

(ii) Point contact situations

Situations which could lead to intense local deformation are illustrated in figure 27 (c) to (f). Figure 27 (c) and (d) represent the case when a hard particle indents a softer one. This would arise when there is more than one type of explosive or when grit particles are present. The process is similar to microparticle impact, and again it is possible for conditions favourable for adiabatic shear failure to arise. If there is a shear force as well as a normal force a ploughing action could take place. Localization will also occur if the 'point' is soft: Yuill (1953) has shown that a liquid explosive can be initiated when a sharp metal point is stabbed through it on to a rigid plate. The temperature rise of the needle resulting from its plastic flow was sufficient to initiate the explosive. A similar situation could occur on a microscopic scale inside an impacted explosive compact (figure 27 (e) and (f)). Shearing movements would enhance this effect.

(iii) Flow around sharp points

When a hard angular particle is embedded in a 'sea' of softer material undergoing shear deformation, flow concentrations will occur where the soft explosive flows past sharp points on the grit. This situation is similar to that illustrated in figure 27(j).

(iv) Spalling

If a cavity exists in an explosive through which a shock wave is passing, spalling can occur. The process, which is illustrated in figure 27 (k) to (m) involves the breaking off of a fragment of explosive from one side of the cavity and its impact on the opposite side. On impact the situation will be similar to that occurring in microparticle impact, also to that represented in figure 27(c). This mechanism is similar to that suggested by Blackburn and Seely (1965) to explain the initiation of PETN by high strength shocks.

(v) Viscous effects

Some explosives melt before they explode and in these cases the final stages of heating could take place as a result of viscous flow in the liquid phase. Heavens and Field (1974) have recently obtained photographic evidence of melting occurring in secondary explosives during 'drop-weight' impact. Rideal and Robertson (1948) have suggested that if melting takes place, then flow of the liquid between grains produces hot spots by viscous heating. This process is illustrated in figures 27 (h) and (i) and could occur when grains are sheared against one another or impacted together normally.

(vi) Frictional heating

Much theoretical and experimental work has been done to show that high local temperatures can be produced by friction (see for example, Bowden and Tabor, 1954, 1964, and Highway and Taylor (1966)). Also Bowden, Stone and Tudor (1947) have shown that frictional heating can lead to the initiation of some explosives. Basically, frictional heating will involve a combination of the processes discussed above. The present work supports the view that flow processes are more important in frictional initiation than for example, fracture processes which also take place when brittle materials slide in contact.

## General Discussion

The present experiments also have relevance to earlier studies of initiation. The work of Belajev and Chariton (1936) showed that the explosion of a lead azide crystal produced many high velocity fragments which could ignite another crystal at quite large distances away. The fragments from a 2mg crystal will ignite another ~25mm away in air and 300-400mm away in vacuum. Courtney-Pratt and Rodgers (1955) performed experiments which proved that initiation was by particle impact and not by ultra-violet radiation emitted from the explosion of the first crystal. The particles which caused initiation were ~1μm in diameter and the energy was thought to be caused by a combination of the kinetic energy of impact and exothermic decomposition energy from the reacting particle.

In the experiments in which the electrostatic method of firing was used (figure 20) 1μm particles did not cause initiation up to velocities of ~800ms$^{-1}$. Since the particles in the present experiments were inert and so only provided kinetic energy to the sample it supports the view of Courtney-Pratt and Rodgers that the exothermic energy of the impacting fragments in their experiments was important.

The work of Bowden, Yoffe and their co-workers (1952, 1958) provides evidence that 'hot spot' sizes for many explosives need to be 0.1 to 10μm in diameter (the precise value depending on the temperature and duration of the 'hot spot'). The present work supports this view since initiation was not recorded with particles of a few microns, but only when particle sizes exceeded ~40μm. It is only when particles exceed this size that the regions of intense local plastic deformation are likely to reach the sizes suggested above for 'hot spots'. Unfortunately, it was not possible to project the small particles with velocities above ~1000ms$^{-1}$ and at this velocity the particle energy was only about 25% of that of the large particles moving at 200ms$^{-1}$. Experiments with very high velocity sub-micron sized particles would provide an interesting method for assessing 'hot spot' sizes.

## Conclusions

If 'hot spots' are to be produced in an impacted explosive mechanisms must exist for localized dissipation of the impact energy. From experiments on compacted explosives it is difficult to unambiguously confirm or reject any of several possible initiation mechanisms. In this report experiments have been described in which silver azide crystals were impacted by spherical particles. The stress system produced here is such that no significant fracturing occurs. The fact that no discontinuities are produced in the deforming region restricts the possible basic mechanisms of localization of energy to one, namely plastic deformation. It is shown that at high strain rates silver azide would be expected to deform in localized bands because of temperature softening. Silver azide melts before it explodes and the final stages of the heating must take place while the material is in the liquid phase. It is argued that the bands of molten explosive must initially be very thin and therefore continue to absorb a significant amount of energy. Since the results of the single crystal impact experiments described here give clear evidence in support of this mechanism, it seems likely that the process is also possible with compacted explosives. The result that compacts and single crystals of silver azide have similar threshold conditions, suggests that similar factors control initiation in the two cases. It is clear that in compacted explosives

there are many situations which could lead to localized plastic deformation during impact loading. As a method of assessing the impact sensitivity of explosives generally, the method has a number of advantages over previous methods. It gives a well defined and reproducible impact situation which enables 'post mortem' examination of the impacted region. When the explosive is effectively 'massive', the size and shape of the sample do not affect the impact conditions. The method also gives results on critical particle sizes and velocities required to cause initiation and this has relevance to various practical situations.

## 3. Multiple Shock Experiments

When a solid reactive material is subjected to a shock which is below the critical strength to cause initiation the state of the material can be changed in various ways. For example the shock could cause fragmentation of the grains of the explosive and this could affect the sensitiveness of the material by producing (i) a larger surface to volume area (ii) new surfaces which may (for a short time at least) be more reactive and (iii) gaseous decomposition products as has been shown by earlier work (see Bowden et al (1968), Fox and Soria-Ruiz (1970), previous years' reports.) It is also possible to imagine processes which would decrease sensitiveness; this would be particularly likely in explosive materials which exhibit "dead-pressing".

In a series of experiments we have placed powdered PETN in a specially constructed steel chamber with PMMA windows. The purpose of the windows is to allow high-speed photographic sequences to be taken. A schematic diagram of the experimental arrangement is shown in figure 28. The explosive (E) was PETN of particle size $\sim$ 200$\mu$m diameter packed to a density of 0.88gm.cm$^{-3}$ (i.e. half the single crystal density). The explosive was confined by 5mm thick steel plates (S) sandwiched between 25mm thick PMMA plates. The three plates were bolted together. D were small detonators which could be fired with a predetermined delay and B were barriers. Preliminary experiments were first made to determine the barrier thickness for which a detonator (only one fired) did not cause initiation. Experiments with two shocks of chosen size (both individually sub-critical) could then be made. A Beckman & Whitley (Model 189) framing camera was used to film the events at 2 x 10$^6$ f.p.s. Records were taken both with and without external illumination.

### (a) Experiments with a single detonator.

The strength of shock from a single detonator into the sample was $\sim$ 2kbar. When it passed into a sample of PETN with 4mm between the barriers there was no initiation. However, when the inter-barrier distance was reduced to the range 1.5 to 1.0mm, and the far barrier was a thick steel plate, initiation took place. These results are interpreted as follows. The $\sim$ 2kbar shock enters the PETN but then attenuates. Attenuation would be significant in the powdered PETN of density 0.88 gm.cm$^{-3}$ even over a distance of a few millimeters. When the shock reached the far barrier it would reflect. The reflected shock from the steel barrier would be another compression wave. This would reinforce the initial shock near the barrier where the shocks overlapped. Apparently when the depth of PETN is greater than 1.5 this is not enough for initiation. However, in the range of thickness 1.5 to 1.0mm the initial shock will not have attenuated so much as for greater depths and with the addition of the reflected shock the pressure is sufficient for initiation.

### (b) Experiments with two shocks together.

In these experiments the shocks entered the PETN samples from both ends. The shocks were both of strength $\sim$ 2kbar. When the barrier separation was

4mm, initiation took place. Photographic records taken at 0.53μs frame interval showed initiation taking place near both barriers (note not at the mid-point between the barriers). The time interval between the shocks entering and initiation occurring was ∿10μs.

The time for the passage of a shock through 4mm of PETN would be about 3μs. It is clear therefore that several reflections must have taken place before initiation. The pressure near the barriers after ∿3 reflections is unlikely to be greater than the pressure when the two shocks first reinforce at the mid-point. This experiment therefore gives a strong suggestion that the first passages of the shocks cause sensitisation.

(c) Experiments with the two shocks delayed.

In these experiments the two ∿2kbar shocks were passed with a time interval, t, between them; t was varied between 0 and 0.1s ($10^5$μs). For values of t in the range 0-10μs initiation always occurred, for t between 10-15μs initiation sometimes took place. For t > 15μs no initiation of fast reaction was observed.

(d) Conclusion.

The above experiments taken together show that two sub-critical shocks can cause initiation. These shocks can come from separate sources, or from one source with the second shock produced on reflection at the confinement (if of high acoustic impedance).

When the added shock strength is still sub-critical the shocks may still cause initiation at a later stage after multiple reflections. It is suggested that this is because the PETN is sensitized by the passage of the primary shocks. This sensitisation is relatively short lived, lasting in the present experiments for up to ∿15μs.

## 4. Thermal Decomposition of PETN

Introduction.

Pentaerythritol tetranitrate (PETN) is a widely used secondary explosive. Its relatively high chemical stability allows it to be manufactured, handled and stored with comparative safety. Andreev and Kaidymov (1961) have studied the thermal decomposition of PETN and found that the vapor phase is the least stable. They also showed that the decomposition is greatly affected by the presence of water vapor and slightly by the presence of oxygen. Their value for the activation energy, E, for the decomposition of solid PETN lay between 51.5 - 62.8 kcal $mole^{-1}$ but was based on a limited amount of data. Values from other workers, found using a variety of methods, fall reasonably closely together. Rogers and Morris (1966) using the differential scanning calorimetry technique found a value for E of 47.3 kcal $mole^{-1}$. Soria-Ruiz (1969) obtained 42 kcal $mole^{-1}$ by monitoring the peak m/e 28 using a quadrupole mass spectrometer. Vapor phase decomposition was studied by Robertson (1948) who found E to be 47 kcal $mole^{-1}$. Maycock and Verneker (1970) used thermobarogravimetric techniques and obtained 45 kcal $mole^{-1}$. Most workers agree that the decomposition is complex and takes place concurrently with sublimation. Decomposition products at 210°C were analysed chemically by Rideal and Robertson (1948) who found that the products in a closed system were given by the equation

$$C_5H_8N_4O_{12} = 0.52NO_2 + 2.11NO + 0.42N_2O + 0.07N_2 + 0.28CO_2 + 0.93CO + 0.09H_2$$

$$+ \text{water} + \text{formaldehyde} + \text{residue}.$$

The present work was undertaken to reinvestigate the decomposition but this time using an ultra high vacuum system and analysing the products using a time-of-flight mass spectrometer. 13

## Experimental

PETN in powder form was obtained from E.R.D.E., Waltham Abbey. It was then recrystallized twice from A.R. acetone solution by slow evaporation. The resulting crystals were white, transparent and exhibited semiregular hexagonal shape. Large single crystals of up to about 3 x 5 x 20 mm in size were obtained by this method. Cleavage planes were found to be parallel to the hexagonal faces. Small crystals of about 0.2mg were cleaved from the as-grown crystal. Only freshly cleaved material was used for the decomposition study.

A six-way stainless steel reaction chamber had one end attached to a conventional ultra high vacuum system and the other connected to the flight tube of a Bendix RGA-IA Time-of-flight mass spectrometer (Figure 29). The ion source was ∿40mm away from the site where reaction took place. A small furnace made up of a cylindrical silica tube surrounding a tungsten coil of 0.13mm diameter had a small glass reaction vessel (5mm outside diameter) situated vertically along its axis. A Pt - (Pt, 13% Rh) thermocouple was in contact with the bottom of the reaction vessel. Electrical connection into the vacuum system was made possible by means of a feed-through connection at the bottom end of the reaction chamber. Temperatures of up to ∿ 300°C with an accuracy of ± 0.5°C could be achieved. The PETN crystals were kept in a stainless steel tray, ∿140mm above the reaction vessel, during the system bake-out at 150°C. The section containing the sample was not baked and was kept below 40°C. The stainless steel tray was attached to a linear motion drive so that it could be translated horizontally into a vertical glass tube through a hole in its side. A metal plate with slider, on the other side of the tubing, allowed the tray to pass through but pushed the crystal until it fell to the reaction vessel through the glass tube. The crystal thus only entered the reaction vessel when the conditions for an experiment were favorable.

The furnace was outgassed at 300°C with the system baked-out overnight. With the system cooled to room temperature, the ion gauge kept at 0.4ma emission current, the furnace turned down to the desired temperature and the valve leading to the ion pump closed, the total pressure of the system reached a final value between 1 x $10^{-8}$ to 1 x $10^{-7}$ torr. A glass window in front of the reaction chamber enabled a direct view of the specimen while the reaction was carried out.

In the isothermal decomposition experiment, the total pressure was measured by the ion gauge on a Varian chart recorder, Model G14. For other experiments the specimen was heated from room temperature at a linear rate of 20 degrees per minute. This was achieved by a stepwise increase of the furnace current. From the pressure values the rate of increase in pressure at various temperatures was obtained. In order to analyse the decomposition products, the valve leading to the ion pump was adjusted so that the total pressure in the system during maximum decomposition was maintained within the pressure range $10^{-6}$ to $10^{-5}$ torr. The spectrum was taken at 70eV from a display on a Tektronix oscilloscope Model 7603 using a polaroid camera Model C27.

## Results

The thermal decomposition of PETN was studied below its melting point of 141°C. Isothermal pressure-time curves taken at 80, 88 and 110°C are shown in figure 30. At each temperature the pressure rises rapidly in the initial stage and then decelerates; in the case of curve C the pressure increases again after ∿90 minutes. The pressure-time curve taken at 53°C is shown in Figure 31.

TABLE 4

Distribution of Decomposition Products at Various Temperatures as Revealed by Mass Spectrum

| m/e | Relative Abundance (% of total) | | |
|---|---|---|---|
| | 94.2°C | 125.9°C | 156.1°C |
| 12 | 3 | 0.5 | 2.5 |
| 13 | 0.5 | 2 | 1 |
| 14 | 5 | 3 | 3 |
| 15 | 1 | 1 | 1 |
| 16 | 5 | 4 | 3.5 |
| 17 | 1 | 1 | 3 |
| 18 | 3 | 4 | 12 |
| 19 | 0.5 | 0.2 | - |
| 20 | 1 | 0.5 | - |
| 24 | 1 | 1 | 0.5 |
| 25 | - | 1 | 0.2 |
| 26 | 2.5 | 2.5 | 1.5 |
| 27 | 5 | 5.0 | - |
| 28 | 12 | 9 | 31 |
| 29 | 6 | 11 | 4 |
| 30 | 22 | 20 | 8 |
| 31 | 3 | 3 | 1 |
| 37 | - | 1 | - |
| 38 | 1 | 1.5 | - |
| 39 | - | - | 1 |
| 41 | - | - | 2 |
| 42 | - | 2.5 | - |
| 43 | 0.5 | 1 | 0.5 |
| 44 | 1 | 6 | 12 |
| 46 | 11 | 4.5 | 4.5 |
| 55 | 1 | 4 | 1 |
| 56 | 2.5 | 2.5 | 0.5 |
| 57 | 1 | 2 | 1 |
| 58 | - | 1.5 | - |
| 60 | 1 | 0.5 | - |
| 70 | 0.5 | 0.5 | 1 |
| 71 | - | - | 1 |
| 72 | 0.5 | 1 | - |
| 74 | - | 0.5 | - |
| 76 | 2.5 | 0.3 | 2 |

| m/e | Relative Abundance (% of total) | | |
|---|---|---|---|
| | 94.2°C | 125.9°C | 136.1°C |
| 83 | - | - | 0.2 |
| 85 | 2.5 | 3 | 1 |
| 87 | - | - | 0.2 |
| 89 | 2 | - | - |
| 98 | 3 | - | - |

(Note the increased vertical scale of this figure compared with that of figure 30). At this temperature, there is an initial linear region before the rate decelerates. The final pressure is $1.3 \times 10^{-6}$ torr and is in reasonable agreement with the vapor pressure at the temperature of sublimation as determined by Crimmins (1969). Figure 32 shows an Arrhenius plot of the rate vs. temperature when the specimen was subjected to a linear heating rate of 20 degrees per minute. Two runs A and B were taken by heating up from room temperature and 65°C respectively. An activation energy of 45.9 ± 1.3 kcal $mole^{-1}$ can thus be deduced for run A between 75 and 130°C. Run B becomes parallel to the least squares line of run A. Below 75°C the gas evolution rate is approximately constant. This implies that at low temperature decomposition does not occur. At the completion of the reaction, no solid residue was left behind. It was not possible to detect by visual observation whether surface melting took place during the reaction. However, it was observed that the original transparent sample, when in the reaction vessel, gradually became opaque at its surface as the reaction progressed.

Mass spectra taken at three temperatures (94°, 126° and 156°C) are presented in table 4. The mass spectrum of the decomposition products has major peaks in the low mass region below m/e 50. Prominent peaks are 18, 28, 29, 30, 44 and 46. The distribution is seen to be influenced by the temperature of decomposition. Below the melting point of PETN (141°C) a large amount of m/e 30 is found whereas at higher temperature m/e 18 and 28 dominate. These peaks correspond to the decomposition products: $H_2O$, $N_2$, CO, HCHO, NO, $CO_2$, $N_2O$ and $NO_2$. Because the crystal is recrystallized from acetone some of the trapped solvent also shows up in some of the spectra. The base peak occurs at m/e 43 due to the fragment ion $CH_3CO^+$, but the amount is not significant in comparison with the decomposition products. Over the high mass region (i.e. m/e > 50) prominent peaks occur at 55, 56, 76 and 85.

## Discussion

The thermal decomposition of nitrate and nitrite esters which contain the four elements C, H, N, O is generally a complex series of reactions accompanied by varying amounts of oxidation. For both types of esters the final products are NO, $NO_2$, $N_2O$, CO, $CO_2$, $H_2O$, HCHO, HCN, alcohol and aldehyde (Benson 1960). For mononitrate and nitrite esters, the primary process involves the rupture of the RO-NO bond producing $NO_2$ or NO. The bond dissociation energy is estimated to be in the neighborhood of 41 kcal $mole^{-1}$ (Levy 1954). As $NO_2$ and NO are very reactive radicals, secondary reaction involving these species will take place. For polynitrate esters, it would be interesting to know whether the molecule first breaks down into mononitrate (i.e. breaking of a C-C bond) or whether the decomposition involves the rupture of the RO-NO bond, as in the case of mononitrate esters. Since atmospheric gases such as molecular oxygen and water vapour are known to affect the reaction rate the ideal situation is for the reaction to take place in an ultra high vacuum system. Any adsorbed gaseous species or volatile impurities are then desorbed and the surface of the specimen can be rendered relatively free from contamination which might act as a catalyst.

PETN is a molecular compound in which the molecules are bound by van der Waal's forces. The weak binding energy is reflected in its low melting point (141°C) and high volatility. Several workers (Edwards 1954, Crimmins 1969, Wood 1970) using effusion methods have studied the vapor pressure at different temperatures. The calculated heat of sublimation ranges from 29 to 36.3 kcal $mole^{-1}$. The value of 29 kcal $mole^{-1}$ obtained by Crimmins appears to be the most reliable since measurements were taken at a lower temperature range where decomposition is not significant. Recently Maycock and Verneker (1970) have

studied the kinetics of sublimation by weight loss measurements under a stream of helium gas maintained at a pressure of $5 \times 10^{-2}$ torr. An activation energy of 26 kcal $mole^{-1}$ was deduced and this is in reasonable agreement with the heat of sublimation determined by Crimmins. At $5 \times 10^{-2}$ these workers did not detect an exotherm due to decomposition, but this does not exclude the possibility of limited decomposition taking place in the solid phase or decomposition in the vapour phase. For thermally unstable organic compounds both sublimation and decomposition occur simultaneously. While sublimation is pressure dependent and prevails at low pressure decomposition becomes more important as the temperature is raised.

There has been some controversy regarding the thermal stability of solid PETN. Aubertein (1954) recrystallized PETN twice from acetone and found that while untreated crystals of PETN gave an initial high loss of water and acid, recrystallized material did not decompose significantly when held at 100°C for three weeks. However, Andreev and Kaidymov (1961) using manometric methods, report detecting decomposition beginning at about 80°C. Our isothermal pressure-time curves show different types of behavior depending on the temperature (figures 2 and 3). Furthermore when a sample is heated up at a linear rate of 20 degrees $min^{-1}$ the rate of gas evolution increases exponentially above 75°C. The mass spectrum taken above this temperature revealed large quantities of decomposition products together with some PETN vapor. The decomposition curves in figures 2 and 3 have an initial rapid acceleration in rate which then gradually decreases. In the case of curve C (figure 2), the highest temperature studied, the decrease is followed by a further increase. Levy (1954) has found that $NO_2$ retards the decomposition of ethyl nitrate ($CH_3CH_2O\ NO_2$) while NO accelerates the reaction. These gases are produced in relatively large amounts here and it is possible that the way their relative abundance changes influences the decomposition of PETN.

From the energetic point of view, the primary process in the decomposition of PETN appears to be the rupture of one RO-NO bond followed by the elimination of a neutral formaldehyde molecule.

$$C(CH_2ONO_2)_4 \longrightarrow C(CH_2ONO_2)_3\ CH_2O + NO_2 \qquad (1)$$

$$C(CH_2ONO_2)_3\ CH_2O \longrightarrow C(CH_2ONO_2)_3 + HCHO \qquad (2)$$

It is difficult to know how the nitrate ester radical $C(CH_2ONO_2)_3$ undergoes further decomposition. However, the relatively large amount of $CH_2O\ NO_2$ (m/e 76) peak present in the mass spectrum suggests the ultimate breaking down of $C(CH_2ONO_2)_3$ to give,

$$C(CH_2ONO_2)_3 \longrightarrow 2\ CH_3ONO_2 + 2\ CO + NO \qquad (3)\ T$$

The methyl nitrate, in analogy with the decomposition of $CH_3CH_2ONO_2$, could then undergo the following steps,

$$CH_3ONO_2 \longrightarrow CH_3O + NO_2 \qquad (4)$$

$$CH_3O + NO_2 \longrightarrow HCHO + HONO \qquad (5)$$

$$2\ HONO \longrightarrow H_2O + NO + NO_2 \qquad (6)$$

$$CH_3O + HCHO \longrightarrow CH_3OH + HCO \qquad (7)$$

$$HCO + NO \longrightarrow CO + HNO \qquad (8)$$

$$2\ HNO \longrightarrow H_2O + N_2O \qquad (9)$$

These equations are certainly consistent with our mass spectra results. The rate of determining step is probably equation 1. The calculated activation energy of 45.9 ± 1.3 kcal $mole^{-1}$ agrees reasonably with Levy's result of 42 kcal $mole^{-1}$ for the decomposition of $CH_3CH_2ONO_2$.

The activation energy is close to that quoted by some other workers (Robertson 1948, Rogers and Morris 1966, Maycock and Verneker 1970), who gave values in the range 45 to 47.3 kcal $mole^{-1}$. The close agreement between our value and these other results indicates that the values given by Andreev and Kaidymov (1961) and Soria-Ruiz (1969) are too high and too low respectively.

## Conclusions

The thermal decomposition of PETN has been studied in an ultra-high vacuum system. Isothermal pressure-time curves showed different types of behaviour depending on the temperature; it is possible that the form of these curves depends on the relative amounts of NO and $NO_2$ produced. For samples heated at a linear rate the rate of gas evolution increased exponentially above 75°C. The activation energy for the temperature range 75 to 130°C was 45.9 ± 1.3 kcal $mole^{-1}$. Since the activation energy for the sublimation of PETN is 26 kcal $mole^{-1}$ it is concluded that sublimation is dominant below 75°C, but that above this temperature decomposition takes place as well. The absence of an exotherm in the differential thermal analysis data of Maycock and Verneker (1970) and the presence of decomposition products found by us strongly suggest that decomposition is preceded by sublimation and that it occurs predominantly in the vapor phase.

The magnitude of the measured activation energy supports the view that the primary process in the decomposition is the rupture of one of the $RO-NO_2$ bonds. It is suggested that this is followed by the elimination of a neutral formaldehyde molecule and then breakdown of $C(CH_2ONO_2)_3$ to give $CH_3ONO_2$, CO and NO. Support for this step is given by the mass spectrum which showed relatively large amounts of $CH_2ONO_2^+$ (m/e 76). The remaining steps in the decomposition it is thought follow the pattern established by Levy (1954) for ethyl nitrate.

## References


Afanas'ev, G.T. & Bobolev, V.K. 1961, Dokl. Akad. Nauk SSSR 138, 886.

Afanas'ev, G.T. & Bobolev, V.K. 1971, Initiation of Solid Explosives by Impact. Transl., Israel Program for Scientific Transl., Jerusalem.

Afanas'ev, G.T., Bobolev, V.K. Kazarcva, Yu.A. & Karabanov, Yu.F. 1972, Fiz. Goreniya i Vzryva 8(2), 299.

Andreev, K.K. & Kaidymov, B.I. 1961, Russ. J. Phys. Chem. 35, 1324.

Andreev, K.K., Maurina, N.D. & Rusakova, Yu.A. 1955, Dokl. Akad. Nauk SSSR 105, 533.

Andrianova, G.P., Kechekyan, A.S. and Kargin, V.A., 1971, J. Polymer Sci. A-2, 9, 1919.

Aubertein, P. 1954, Chem. Abstracts 48, 4837b.

Bahrani, A.S., Black, T.J. & Crossland, B. 1967, Proc. Roy. Soc. A296, 123.

Belajev, A.F. and Chariton, J.B., 1936, Acta Phys-Chim. U.R.S.S., 5, 757.

Benson, S.W. 1960, "The Foundations of Chemical Kinetics", McGraw-Hill Book Co., New York.

Blackburn, J.H. and Seely, L.B., 1965, Trans. Farad. Soc. 61, 537.

Bolkhovitinov, L.G. 1959, Dokl. Akad. Nauk SSSR 125, 570.

Bolkhovitinov, L.G. & Pokhil, P.F. 1958, Dokl. Akad. Nauk SSSR 123, 637.

Bowden, F.P. 1950, Proc. Roy. Soc. A204, 20.

Bowden, F.P. 1963, Ninth Int. Symp. on Combustion, p499, Academic Press, N.Y.

Bowden, F.P., Fox, P.G. and Soria-Ruiz, J. 1968, Nature 220, 778.

Bowden, F.P. & Gurton, O.A. 1949, Proc. Roy. Soc. A198, 337.

Bowden, F.P., Mulcahy, M.F.R., Vines, R.G. & Yoffe, A.D., 1947, Proc. Roy. Soc. A188, 291.

Bowden, F.P. and Tabor, D., 1954, 'The Friction and Lubrication of Solids', Pt.I, O.U.P. 1954; 'The Friction and Lubrication of Solids', Pt.II, O.U.P. 1964.

Bowden, F.P., Sone, M.A. and Tudor, G.K., 1947, Proc. Roy. Soc. A188, 329.

Bowden, F.P. & Yoffe, A.D. 1949, Third Symp. on Combustion & Flame Phenomena, p551, Williams & Wilkins, Baltimore, Md.

Bowden, F.P. & Yoffe, A.D. 1952, Initiation and Growth of Explosion in Liquids and Solids, C.U.P.

Bowden, F.P. & Yoffe, A.D. 1958, Fast Reactions in Solids, Butterworth, London.

Brookes, C.A., O'Neill, J.B. and Redfern, B.R.W.,1971, Proc. Roy. Soc. A322, 73.

Carlslaw, H.S. and Jaeger, J.C., 1959, 'Conductivity of Heat in Solids' O.U.P. 2nd Ed. p 263.

Chaudhri, M.M., 1972, Combustion and Flame 19, 419.

Chaudhri, M.M. and Field, J.E. 1974, Proc Roy. Soc. A340, 113.

Chaudhri, M.M., Field, J.E., Heavens, S.N. & Coley, M. 1972, Tenth Int. Conf. on High-speed photography, p472, Nice.

Copp, J.L. & Ubbelohde, A.R. 1948, Phil. Trans. A241, 261.

Courtney-Pratt, J.S. and Rogers, G.T., 1953, Nature 175, 176.

Cowan, G.R. & Holtzmann, A.H. 1963, J. Appl. Phys. 34, 928.

Crimmins, F.T. 1969, Lawrence Rad. Lab. Rep. No. U.C.R.L. 50704, July 1969.

Edwards, G. 1954, Trans. Faraday Soc. 49, 152.

Eirich, F.& Tabor, D. 1948, Proc. Camb. Phil. Soc. 44, 566.

Fox, P.G. 1970, J. Solid State Chem. 2, 491.

Fox, P.G. and Soria-Ruiz, J. 1970, Proc. Roy. Soc. A317, 79.

Garner, W.E., 1958, Proc. Roy. Soc. A246, 203.

Gray, W.A. 1968, The Packing of Solid Particles, Chapman & Hall, London.

Heavens, S.N. 1973, Ph.D. Thesis, University of Cambridge.

Heavens, S.N. and Field, J.E. 1974, Proc. Roy. Soc. A338, 77.

Highway, R.J. and Taylor, D.S. 1966, Wear 9, 310.

Hunt, J.N. 1968, Phil. Mag. 17, 669.

King, R.F. and Tabor, D. 1954, Proc. Roy. Soc. 223, 225.

Kholevo, N.A. 1946, Tr. Kazansk. Khim. Tech. Inst. 10, 91; ibid. 1947, 11, 116.

Levy, J.B. 1954, J. Am. Chem. Soc. 76, 3790.

Linder, P.W. 1961, Trans. Faraday Soc. 57, 1024.

Ljungberg, S. 1958, Nobel Hefte 24, 40.

Mader, C.L. 1965, Phys. Fluids, 8, 1811.

Maycock, J.N. and Pai Verneker, V.R. 1970, Thermochimica Acta 1, 191.

McKenzie, D, and Brune, J.N. 1972, Geophys. J.R. astr. Soc. 29, 65.

Plant, J., 1972, Phys. Bull. 23, 203.

Prandtl, L. 1923, Z. Angew. Math. u Mech. 3, 401.

Recht, R.F. 1964, J. Appl. Mech. 31, 189.

Rideal, E.K. & Robertson, A.J.B. 1949, Proc. Roy. Soc. A195, 135.

Robertson, A.J.B. 1948, J. Soc. Chem. Ind. 61, 221.

Rogers, R.N. and Morris, E.D.Jr. 1966, Anal. Chem. 38, 412.

Roseen, R. 1974, J. Mat. Sci. 9, 929.

Schroeder, W. & Webster, D.A. 1949, J. Appl. Mech. 16, 289.

Shelton, H., Hendricks, C.D. and Weurker, R.F. 1960, J. Appl. Phys. 31, 1243.

Soria-Ruiz, J., PhD Thesis, 1969, University of Cambridge.

Stock, T.A.C. and Thomson, K.R.L. 1970, Metall. Trans. 1, 219.

Taylor, W. & Weale, A. 1932, Proc. Roy. Soc. A138, 92.

Ubbelohde, A.R. 1948, Phil. Trans. A241, 199.

Uetz, E. and Gommel, G. 1966, Wear 9, 282.

Wilson, M.P.W. 1967, PhD Thesis, University of Cambridge.

Winter, R.E. 1971, PhD Thesis, University of Cambridge.

Wood, C.E.C. 1970, PhD. Thesis, University of Nottingham.

Yoffe, A.D. 1949, Proc. Roy. Soc. A198, 373.

Yuill, A.M. 1953, PhD Thesis, University of Cambridge.

Zener, C. and Hollomon, J.H. 1944, J. Appl. Phys. 15, 22.

## FIGURE CAPTIONS

Figure 1. Experimental arrangement at instant of impact. W - drop-weight; G - glass blocks; M - mirrors; S - sample. The upper glass block G is attached to the drop-weight.

Figure 2. Impact of a layer of granular PETN viewed in transmitted light. The sample flows plastically, melts and ignites at a number of sites. The thickness of the layer at the time of ignition is about 50μm. In frames h and i, D is a flaw in the glass surface and I is an ignition site. Mass of sample 14mg. Diameter of field of view 20mm. Interframe time 5.5μs.

Figure 3. Impact of a layer of granular HMX. The sample shows some tendency to flow plastically (frame b) but no melting is observed prior to ignition (frame c). Mass of sample 21mg. Diameter of field of view 20mm. Frame times (μs): a 0, b 50, c 55, d 60, e 65, f 80.

Figure 4. Impact of a layer of granular ammonium perchlorate. The layer becomes transparent (frame b) and subsequently starts to undergo plastic flow (frame c). An ignition site (arrowed), with associated fracturing, appears in frame e, but the reaction fails to propagate. Mass of sample 21mg. Diameter of field of view 20mm. Frame times (μs): a 0, b 75, c 85, d 110, e 180, f 195.

Figure 5. Impact of a layer of blasting gelatine. The sample flows steadily and ignites at grit particles (frames d, e). Mass of sample 25mg. Diameter of field of view 20mm. Frame time (μs): a 0, b 70, c 110, d 150, e 165, f 180.

Figure 6. Impact of a layer of granular PETN containing a grit particle. The sample melts (frame c) and ignites at the ends of the grit particle (frames d, e). Mass of sample 10mg. Diameter of field of view 20mm. Frame times (μs): a 0, b 62.4, c 67.2, d 72, e 76.8, f 81.6.

Figure 7. Impact of a layer of PETN containing 5% paraffin oil. Explosion is initiated close to the periphery (arrowed, frame b) but fails to propagate (frame c). Mass of sample 20mg. Diameter of field of view 20mm. Frame times (μs): a 0, b 95, c 130.

Figure 8. Impact of a layer of HMX containing 2% water. Again localized reaction occurs. Mass of sample 13mg. Diameter of field of view 20mm. Frame times (μs): a 0, b 5.5, c 27.5.

Figure 9. Impact of an annular layer of granular PETN. The air cavity is sealed off (frame b), the sample flows plastically, and eventually melts (frames d to e) and ignites at three sites, one close to the cavity position (frame e). Mass of sample 22mg. Diameter of field of view 20mm. Frame times (μs): a 0, b 16.5, c 44, d 77, e 88, f 93.5.

Figure 10. Impact of an annular layer of HMX. The air at the centre of the sample is not sealed off and compressed, but escapes to the free surface. Mass of sample 18mg. Diameter of field of view 20mm. Frame times (μs): a 0, b 55, c 110.

Figure 11. Experimental arrangement for obtaining pressure-time curves. W - drop-weight; H, R1, R2, R3 - hard rollers; C - cylindrical guiding sleeve; S - sample; G - strain gauge; A - cast steel anvil; D - light detector.

Figure 12. Pressure-time curves for impact of various non-explosive granular samples. (a) no sample (b) TNT (c) ammonium nitrate (d) potassium azide (e) barium nitrate (f) oxalic acid (g) sodium carbonate (h) polystyrene. Mass of hammer 5kg. Drop-height 0.25m (in example (e) the drop-height was 0.5m). Horizontal scale: 100μs/division. Vertical scale: 5mV/division (4.3kbar/division).

Figure 13. Pressure-time curves for impact of RDX. Similar behaviour is shown by PETN, HMX, and ammonium perchlorate. Mass of hammer 5kg. Drop-height (a) 0.35m (b) 0.2m (c) 0.5m (d) 0.25m. Horizontal scale 100μs division. Vertical scale 5mV division (4.3kbar division). The instant of ignition is recorded by the beginning of the light detector pulse in (a), (b) and (c) and by the electrical short-circuit in (d).

Figure 14. Derivation of the pressure-deformation curve for a thin layer during impact.

Figure 15. Impact of a layer of granular potassium nitrate, showing evidence of plastic flow (frames a to h) followed by jetting (frames i to j). Mass of sample 20mg. Diameter of field of view 20mm. Frame times (μs): a 0, b 27.5, c 55, d 82.5, e 110, f 137.5, g 165, h 192.5, i 220, j 247.5, k 275, l 302.5.

Figure 16. (a) Radius of the layer as a function of time during the sequence of figure 15. t = 100μs corresponds to frame e.
(b) Variation of layer thickness during impact as derived from the two experiments. The continuous curve is derived from the R/t curve obtained photographically; the broken curve from the p/t curve for a sample of potassium nitrate.
(c) Pressure-time curve for impact of potassium nitrate.

Figure 17. Radius of a layer of PETN during impact, showing evidence of plastic flow followed by jetting, melting and ignition.

Figure 18. Wave formation in a thin layer during impact (a) RDX (b) annular layer of PETN (c) appearance of waves in PETN after the sample has melted. Diameter of field of view 20mm.

Figure 19. Impact of an asymmetric annular layer of PETN (pressed prior to impact). Ignition occurs prior to melting in the region of unstable flow of material to the right. Mass of sample 20mm. Frame time (μs): a 0, b 55, c 60.5.

Figure 20. Velocities versus particle size for iron and silver spheres accelerated by electrostatic method. Charging surface at $5 \times 10^{8} Vm^{-1}$, accelerating potential 80kV. See Shelton et al (1960), Winter (1971) for details of method.

Figure 21. The explosive driver technique used to accelerate particles in the range 50 - 500um.

Figure 22. A high-speed photographic sequence showing the acceleration of lead particles from a metal plate (lower surface) and their initiation of a silver azide crystal.

Figure 23. The method of mounting the silver azide crystals.

Figure 24. A plastic indentation produced by the impact of an 80um aluminium sphere on a polished silver azide crystal at a velocity of $200ms^{-1}$.

Figure 25. The general positions of shear bands observed by Stock and Thomson (1970) and Wilson (1967), in metal targets impacted by projectiles with spherical tips. The figure also provides a model for calculating the temperatures produced on these bands.

Figure 26. The machining geometry studied by Recht (1964). For the purposes of analysis it is assumed that $V_c$ is approximately equal to the maching velocity.

Figure 27. Situations in which shear concentrations could occur when an explosive consisting of small crystals pressed together (a 'compact') is impacted.

Figure 28. Schematic for multiple shock experiments on powder. E is explosive, SS are steel plates, DD are detonators, and BB are barriers.

Figure 29. Decomposition experiment. S - Tektronix oscilloscope; E - electron multiplier; I - ion source; R - six-way reaction chamber; P - to ion pump; G - ion gauge; C - Varian chart recorder; M - Bendix RGA-1A Time-of-flight mass spectrometer.

Figure 30. Pressure-time curves for isothermal decomposition. Curve A at 80°C; B at 88°C; C at 110°C.

Figure 31. Specific pressure against time; decomposition temperature at 53°C.

Figure 32. Arrhenius plot of the rate of gas evolution. ● heating up from room temperature. ▲ heating up from 65°C.

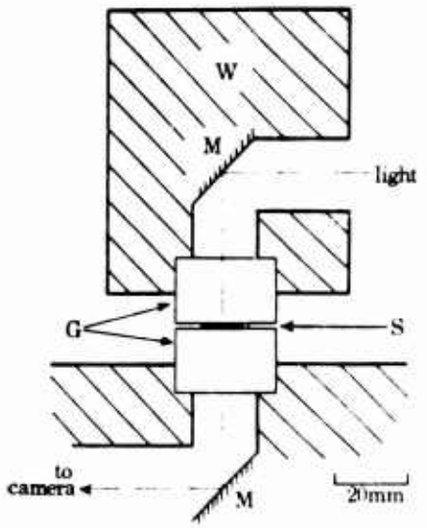
W
M
light
G
S
to camera
M
20mm

1

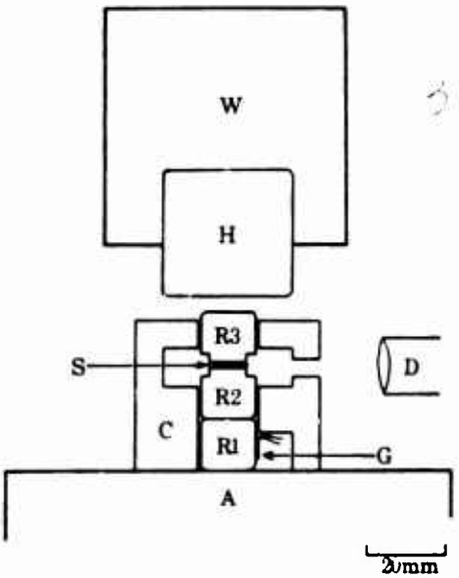
W
H
R3
R2
R1
S
D
C
G
A
20mm

11

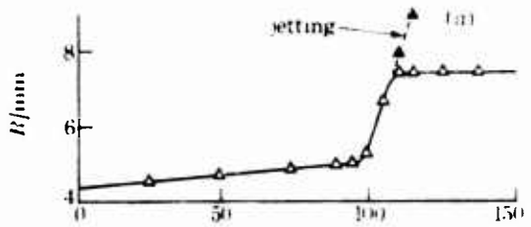
jetting
(a)
h/mm
8
6
4
0
50
100
150

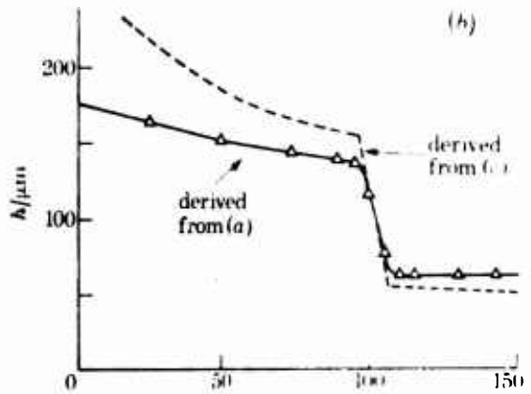
(b)
h/μm
200
100
0
derived from (c)
derived from (a)
50
100
150

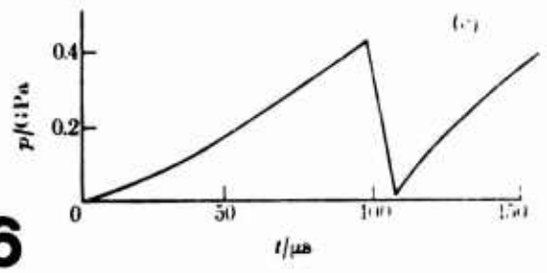
(c)
p/GPa
0.4
0.2
0
50
100
150
t/μs

16

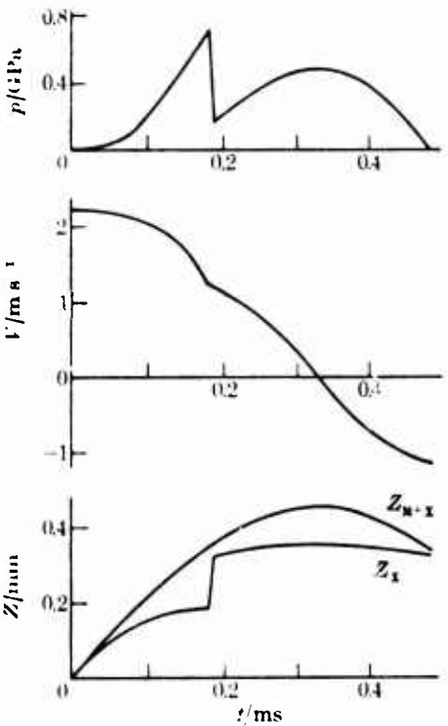
p/GPa
0.8
0.4
0
0.2
0.4
V/m s⁻¹
2
1
0
−1
0.2
0.4
Z/mm
0.4
0.2
0
$Z_{M+X}$
$Z_X$
0.2
0.4
t/ms

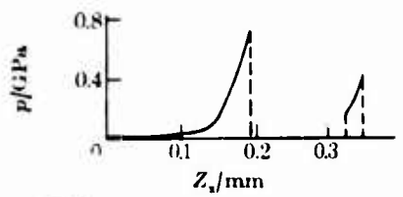
p/GPa
0.8
0.4
0
0.1
0.2
0.3
$Z_x$/mm

14

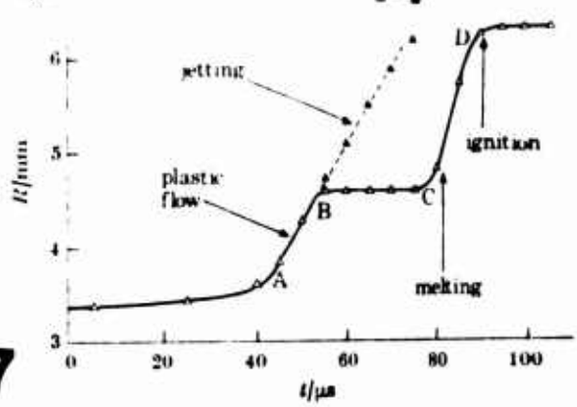
jetting
plastic flow
ignition
melting
A
B
C
D
h/mm
6
5
4
3
0
20
40
60
80
100
t/μs

17

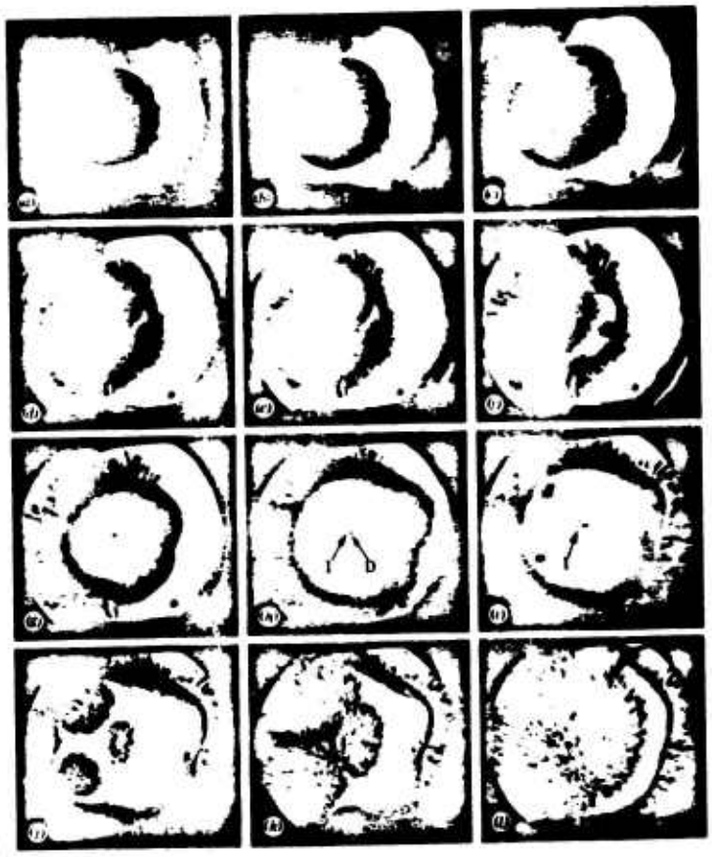

2

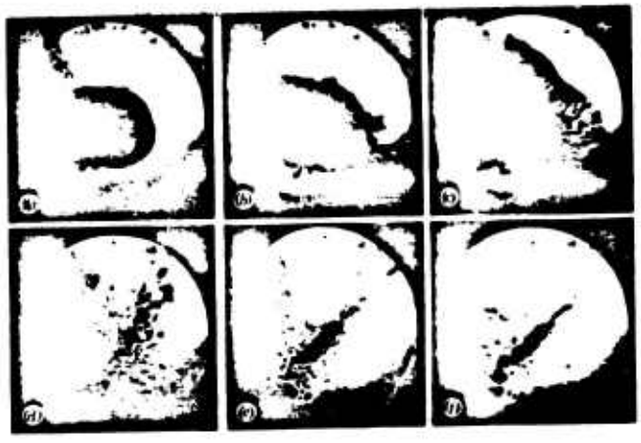

3

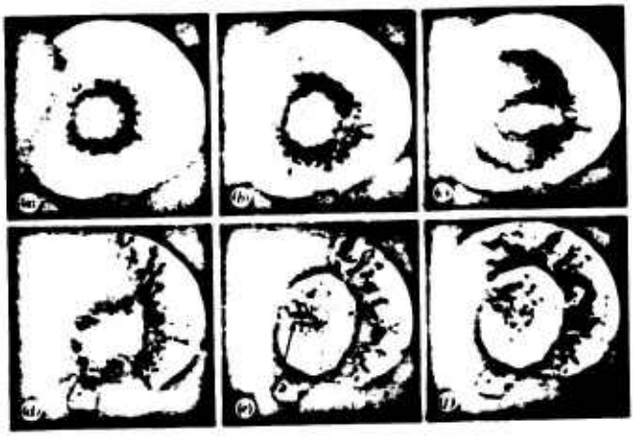

4

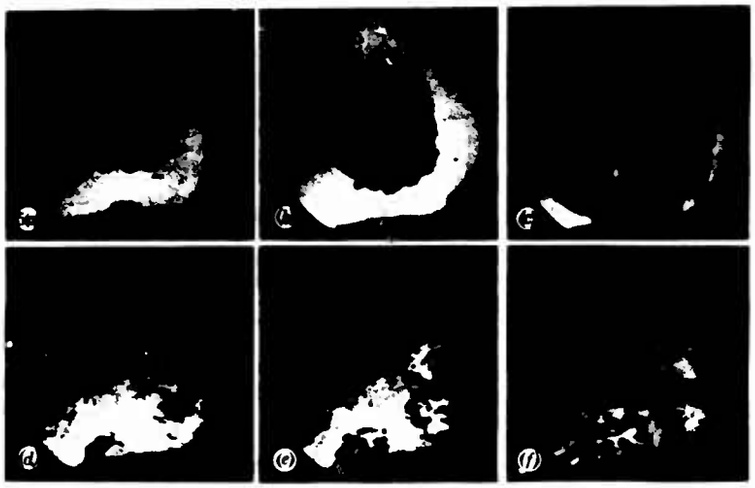

5

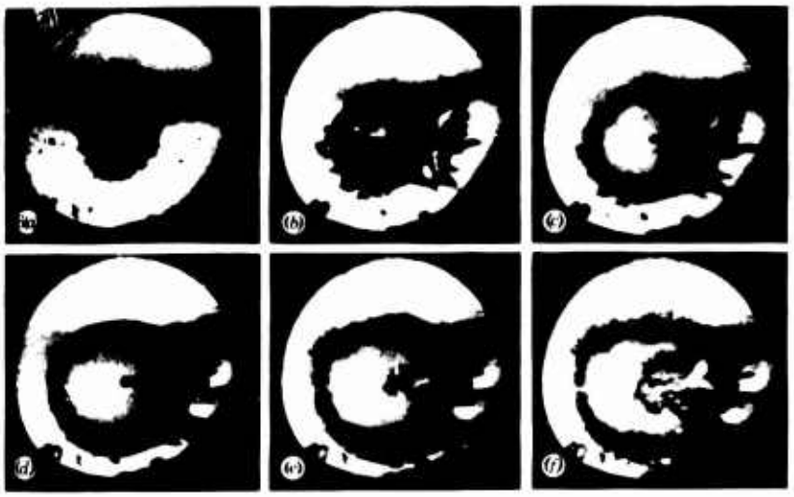

6

7

8

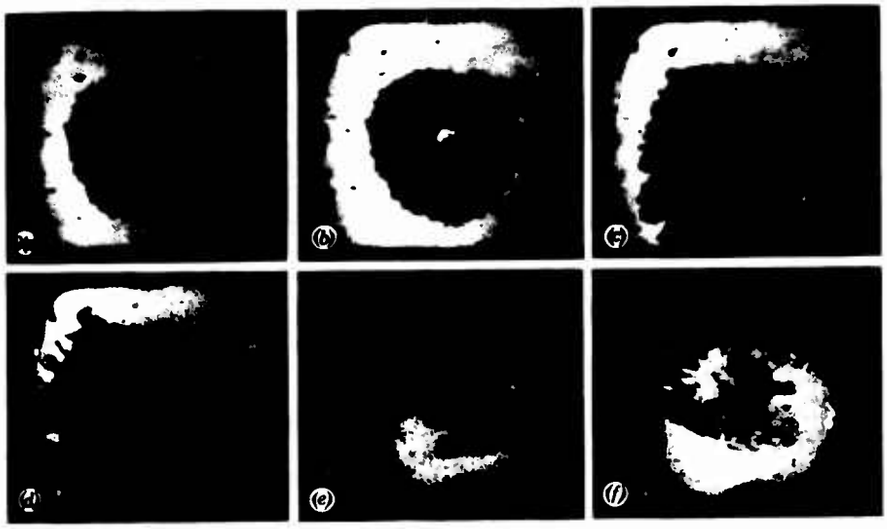

9

10

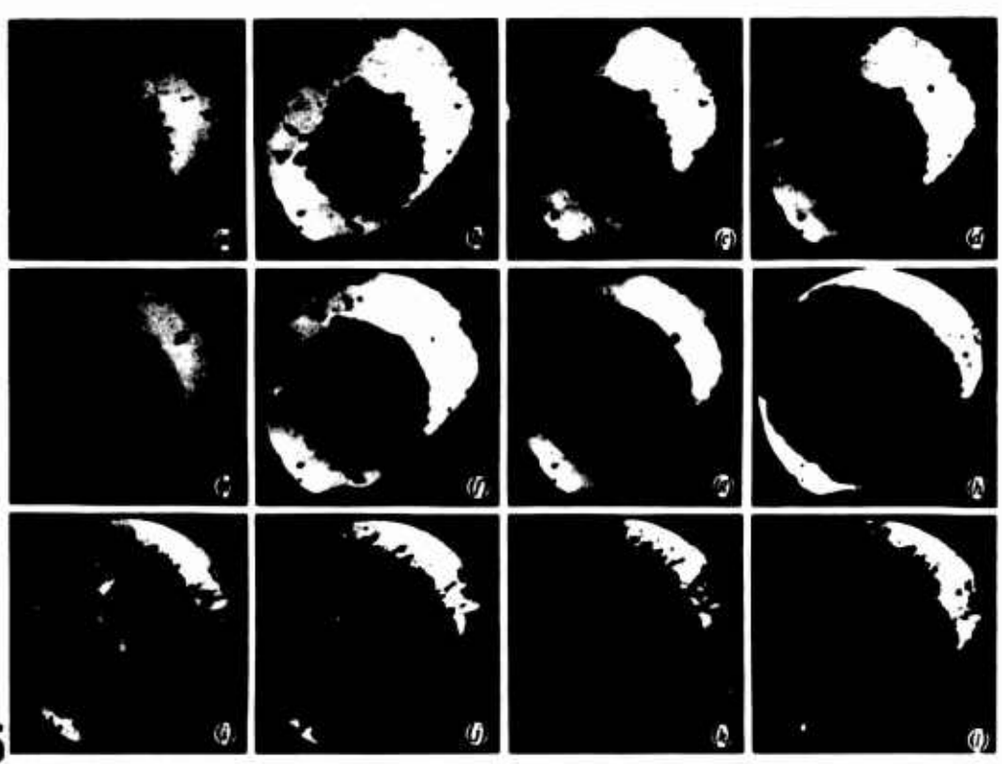

15

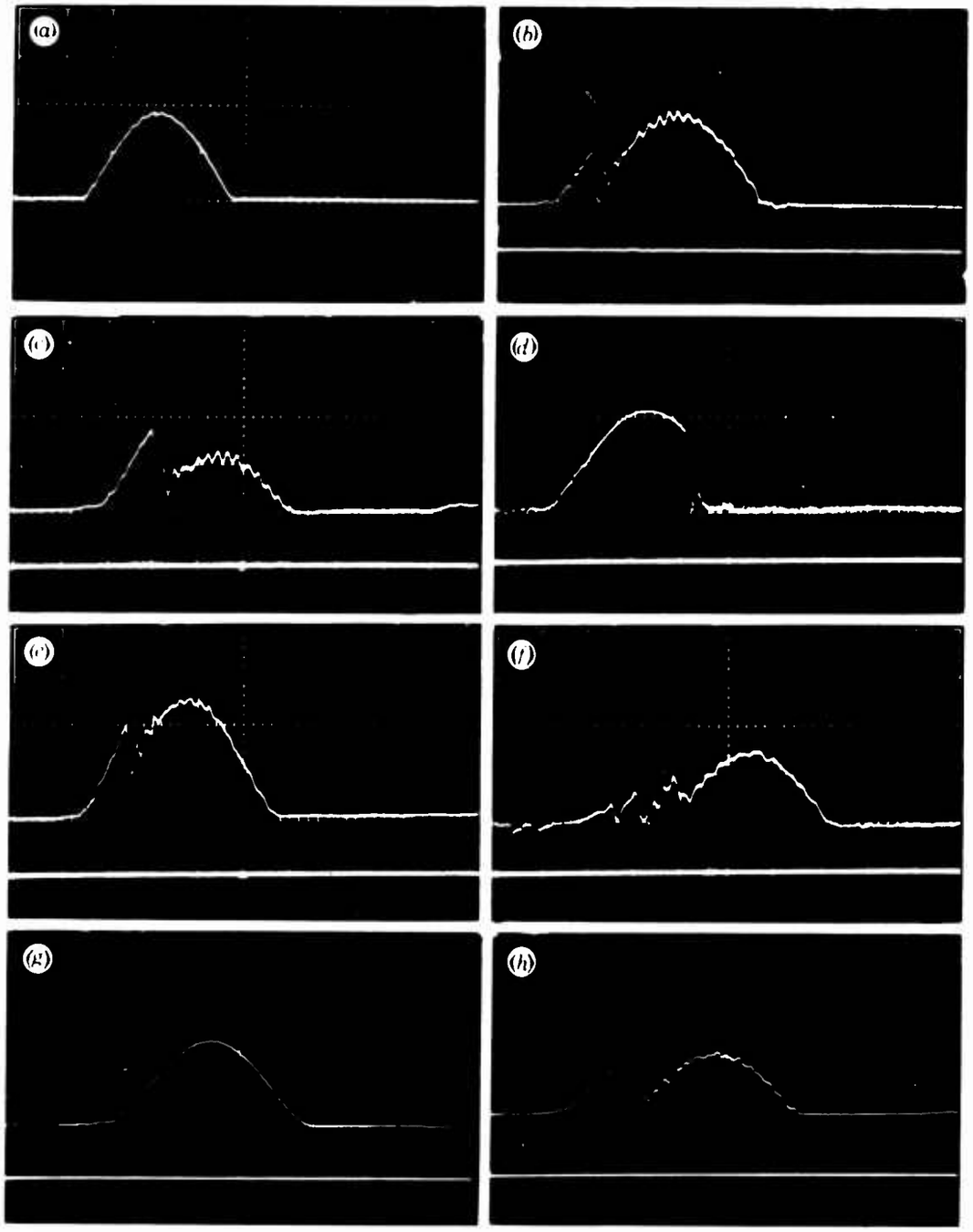


12

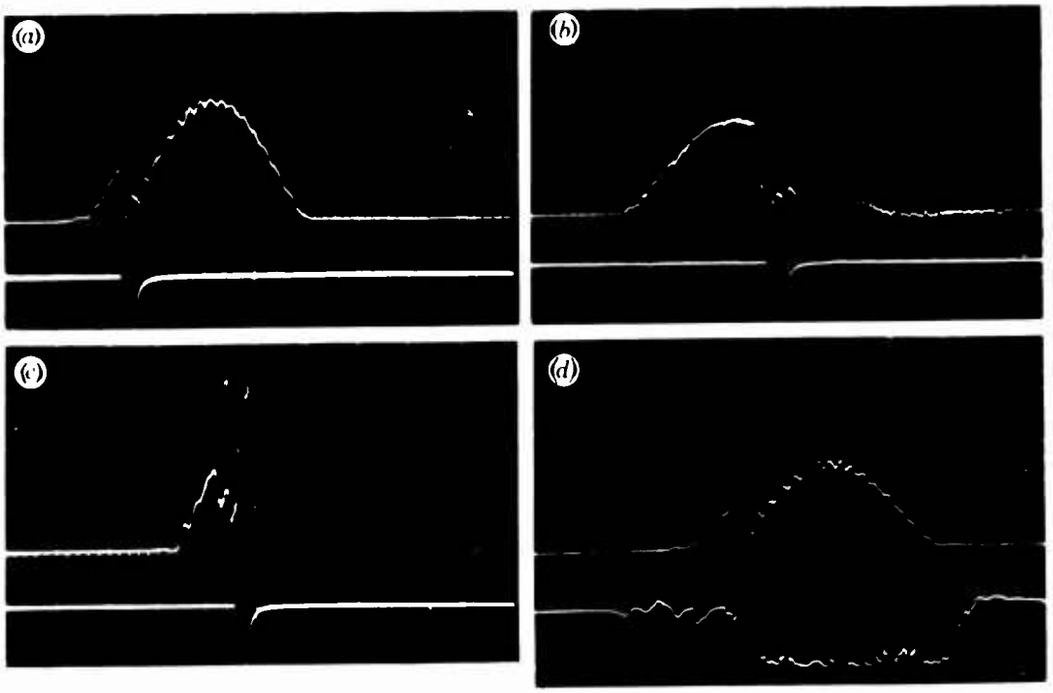


13


18

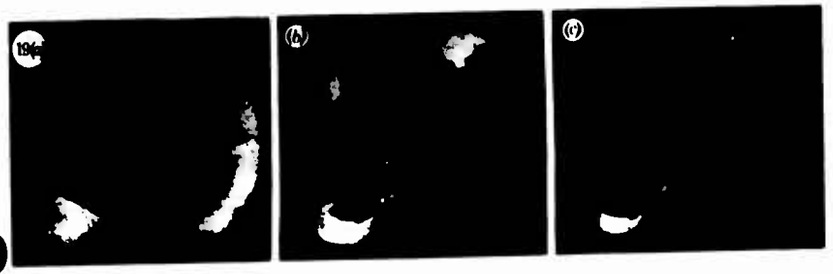


19

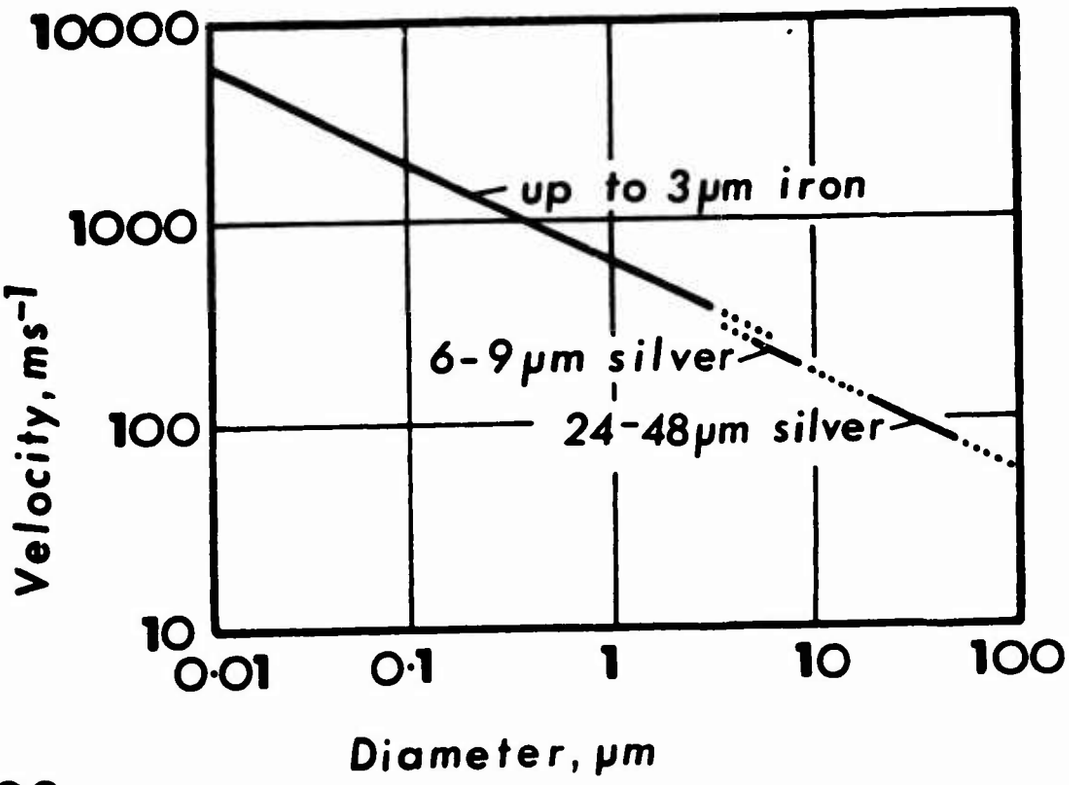
10000
1000
100
10
Velocity, ms⁻¹
up to 3μm iron
6-9μm silver
24-48μm silver
0·01
0·1
1
10
100
Diameter, μm

20

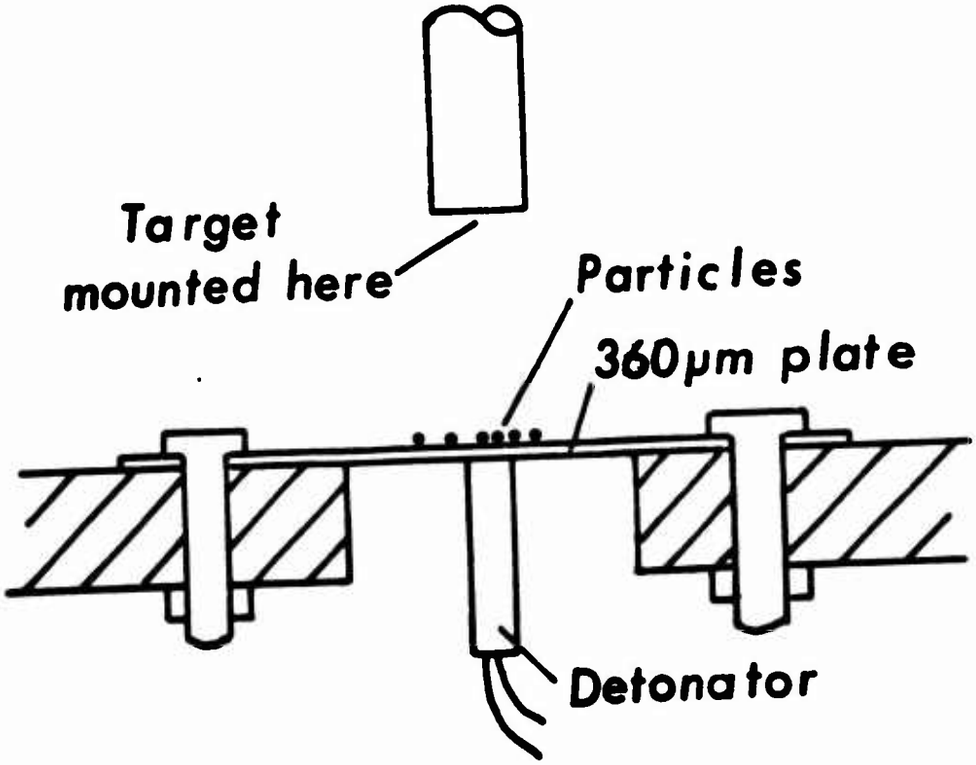
Target
mounted here
Particles
360μm plate
Detonator

21

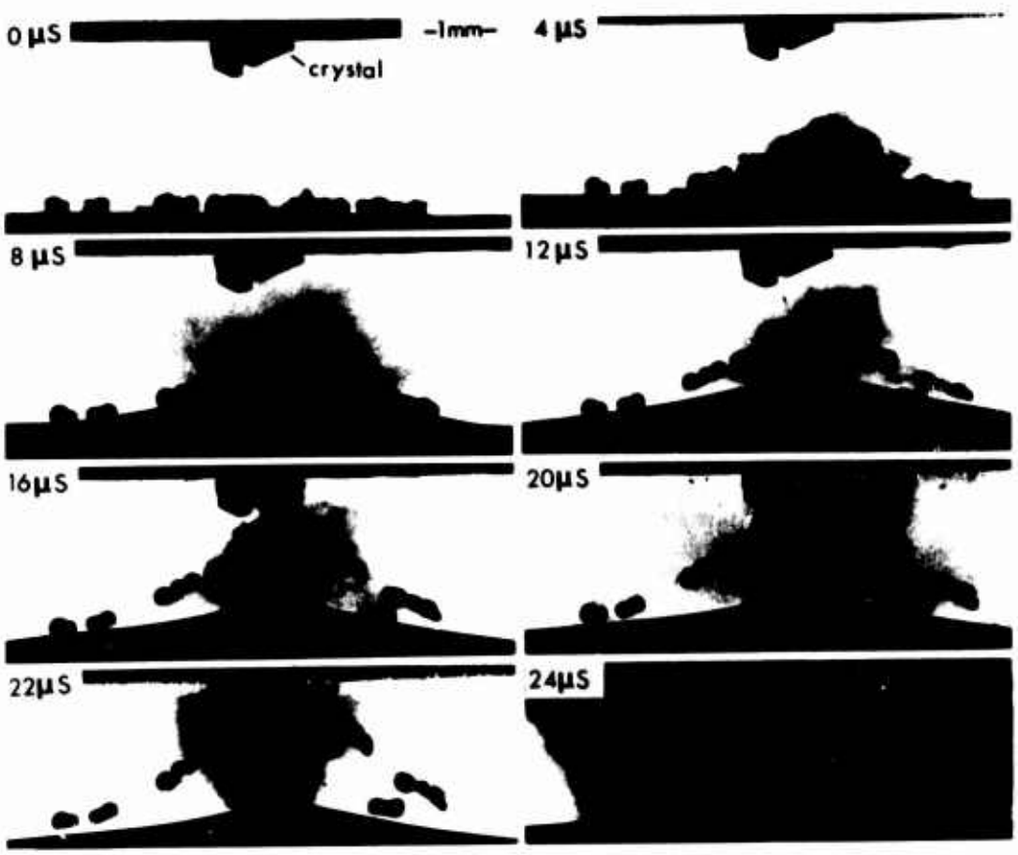


22

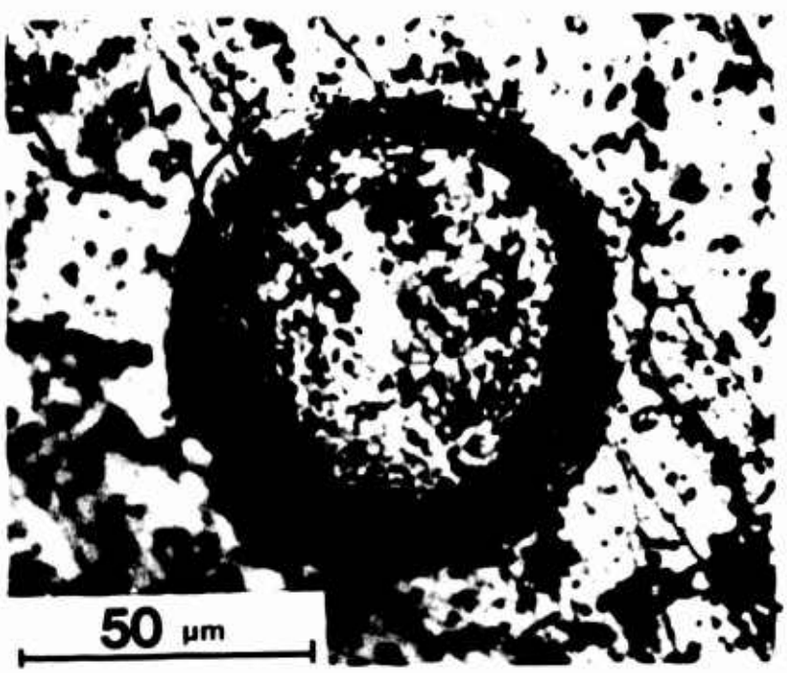


24

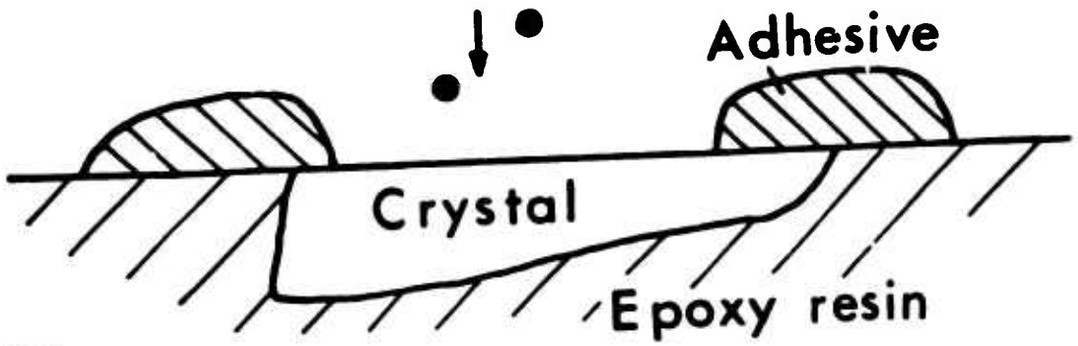
Adhesive
Crystal
Epoxy resin

23

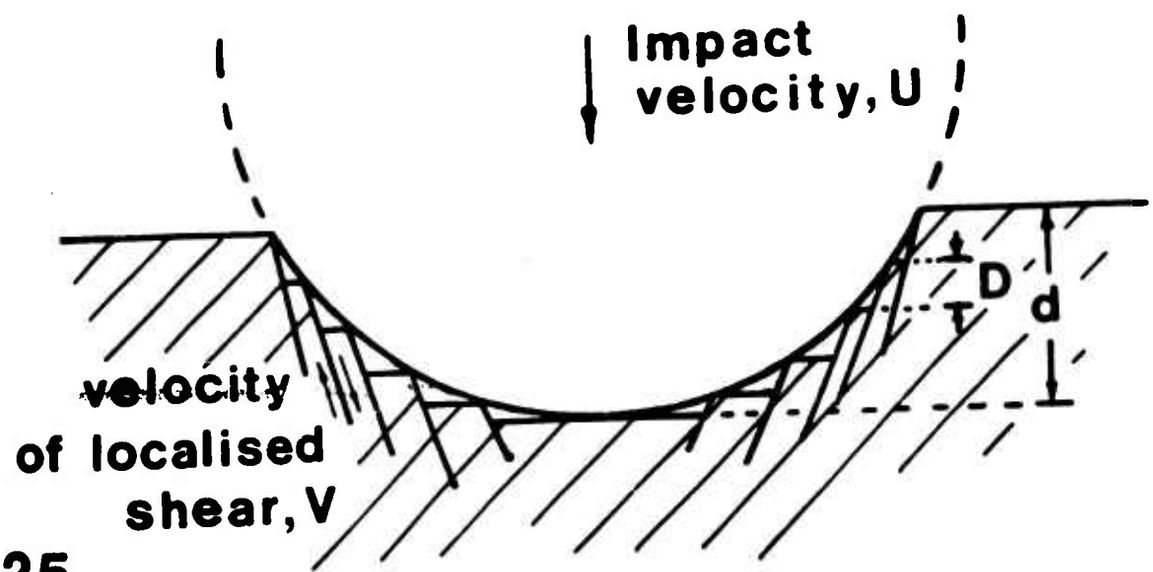
Impact
velocity, U
D
d
velocity
of localised
shear, V

25

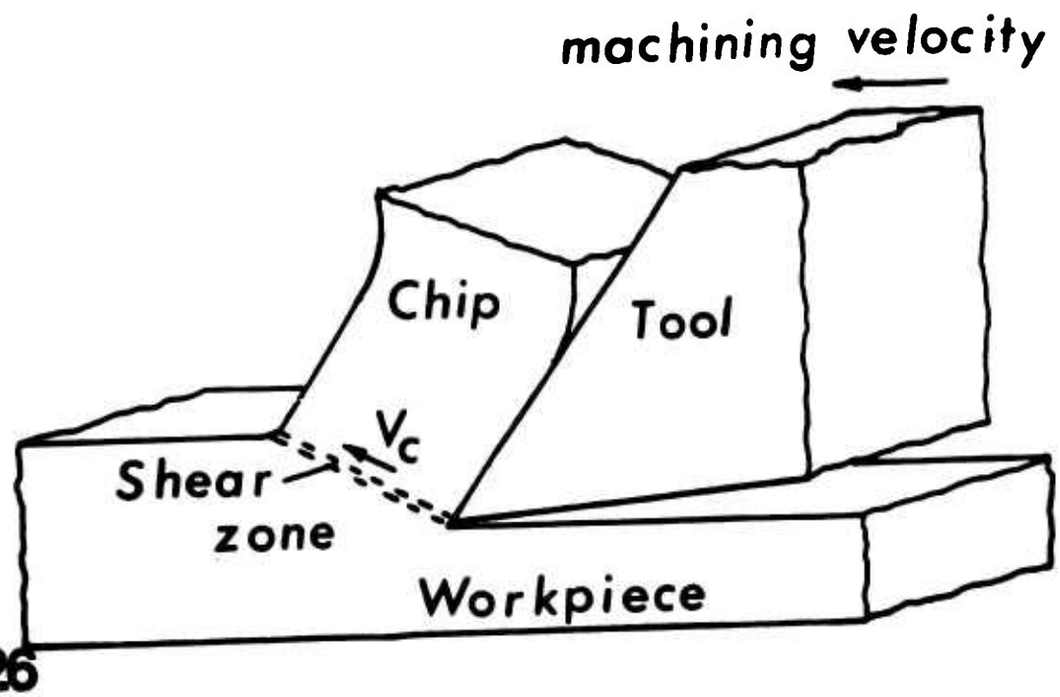
machining velocity
Chip
Tool
Vc
Shear
zone
Workpiece

26

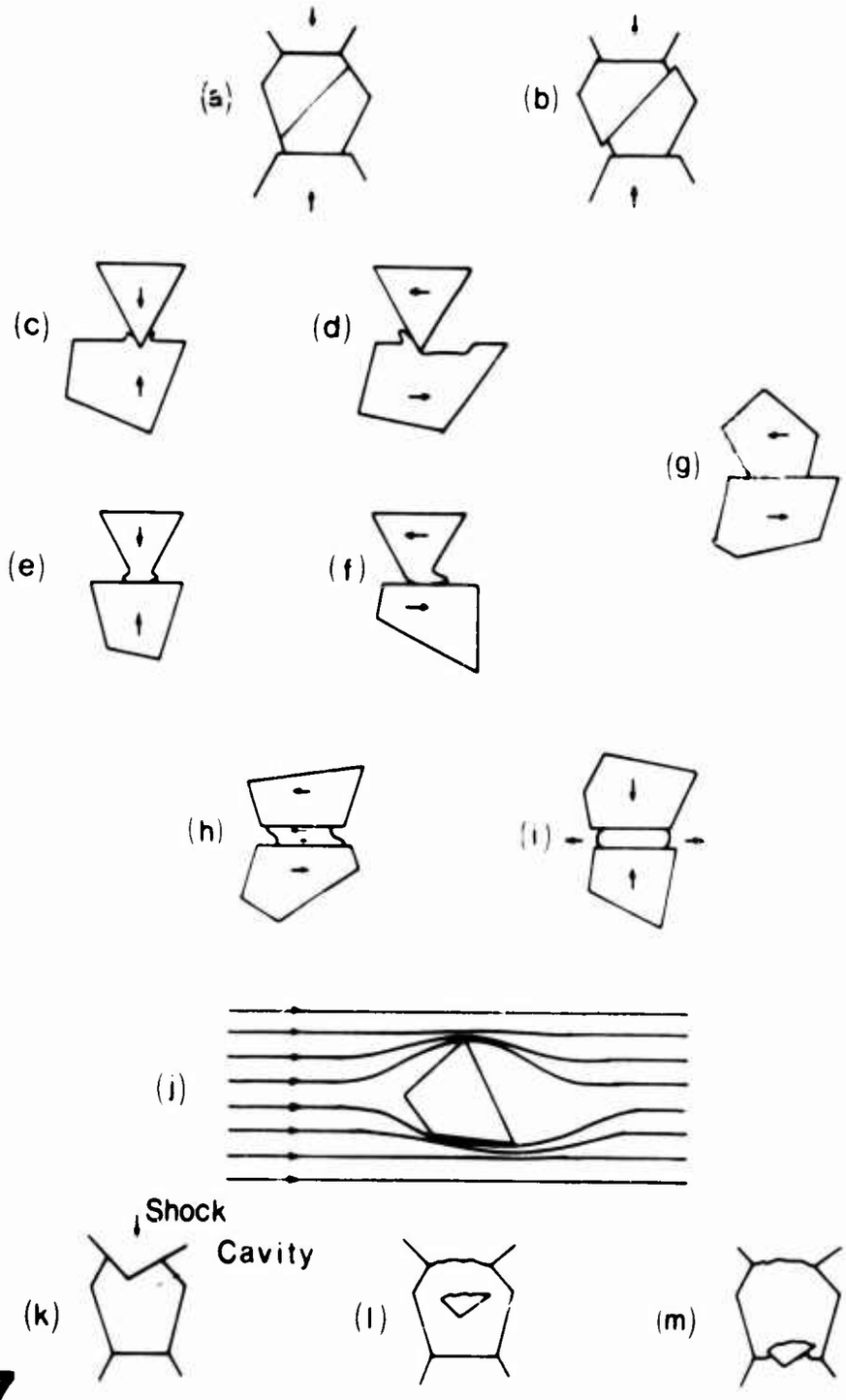


27

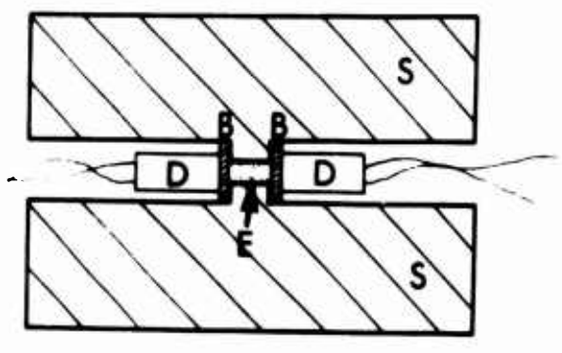


28

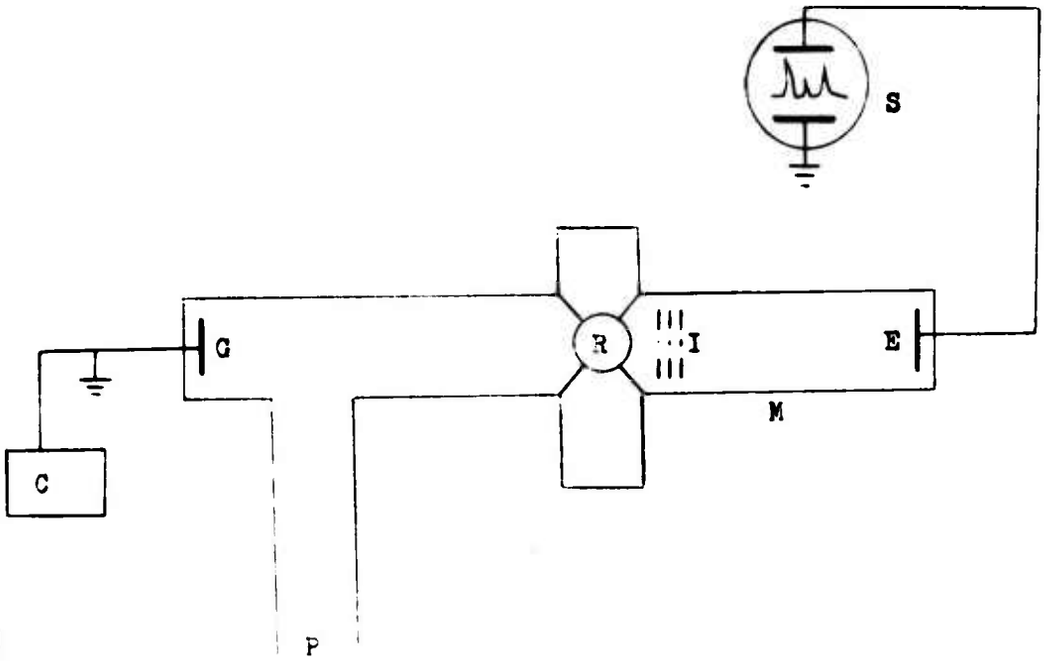
S
G
R
I
E
M
C
P

29

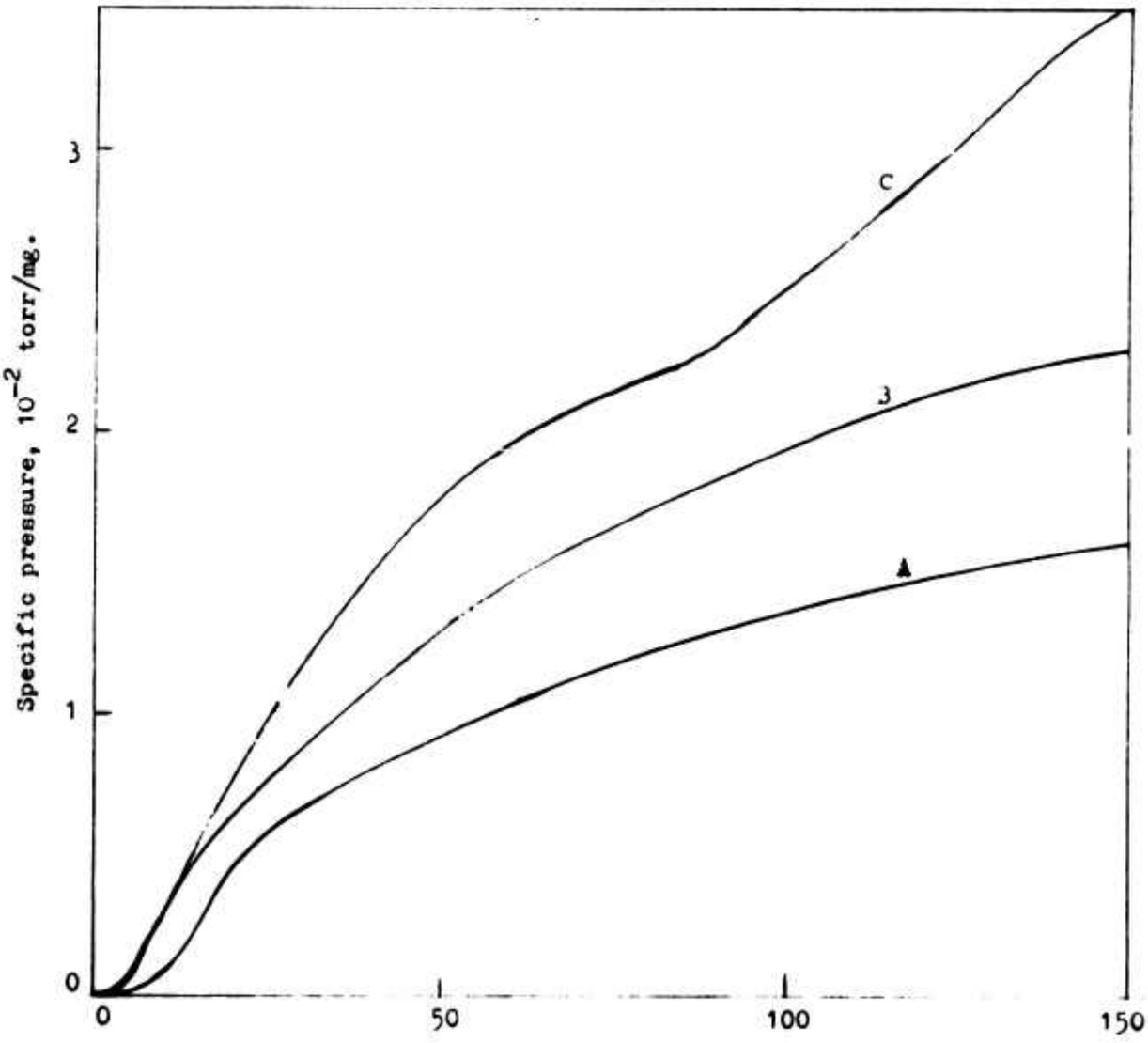
Specific pressure, $10^{-2}$ torr/mg.
0
1
2
3
0
50
100
150
time, min.
C
3
A

30

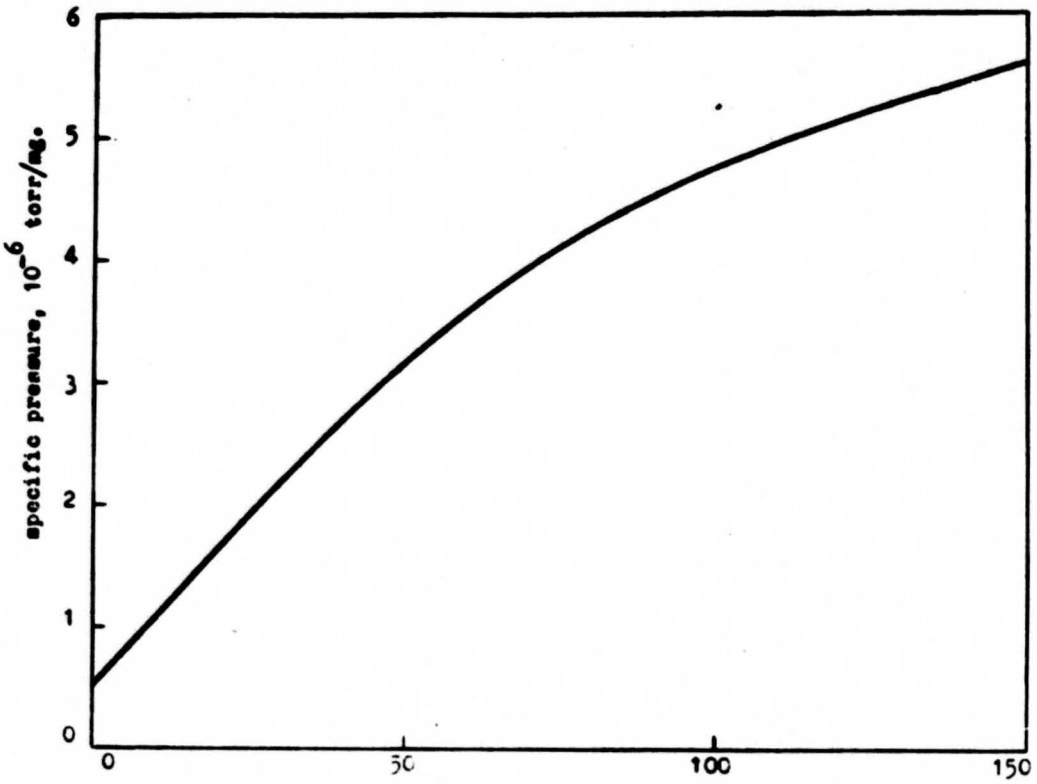
specific pressure, $10^{-6}$ torr/mg.
0
1
2
3
4
5
6
0
50
100
150
time, min.

31

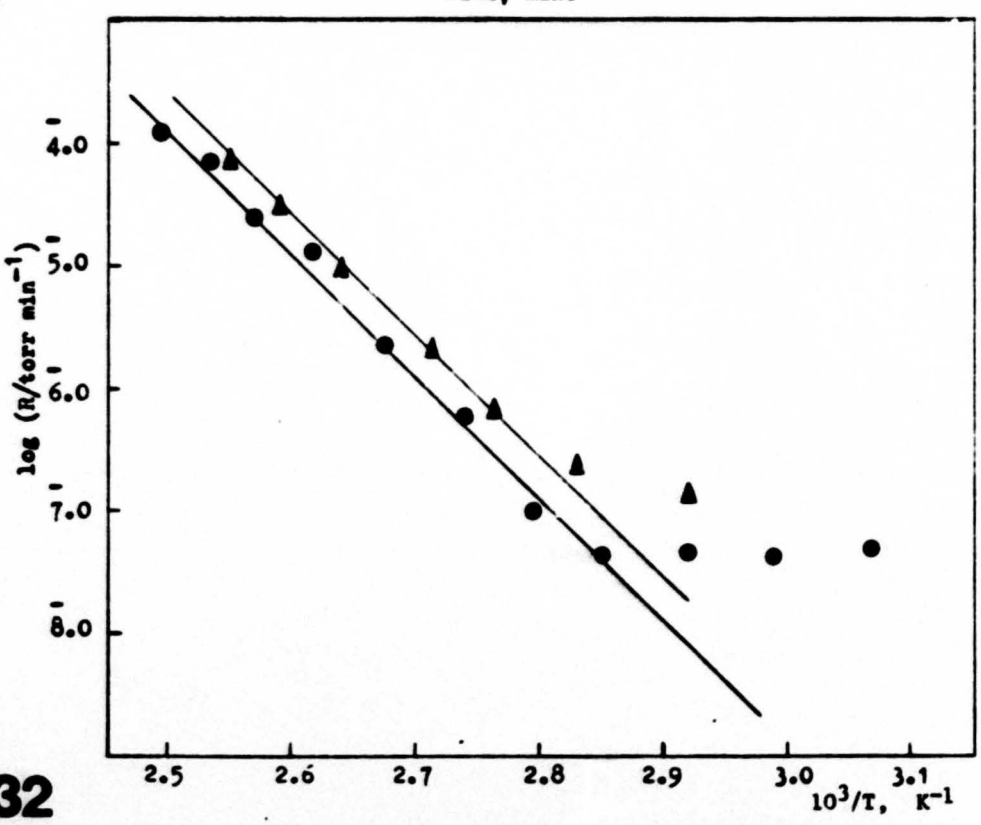
log (R/torr min$^{-1}$)
4.0
5.0
6.0
7.0
8.0
2.5
2.6
2.7
2.8
2.9
3.0
3.1
$10^3/T$, $K^{-1}$

32